

## Microphysical properties of continental clouds from in-situ measurements

A. V. Korolev<sup>1\*</sup>, G. A. Isaac<sup>1</sup>, I. P. Mazin<sup>2</sup>, H. W. Barker<sup>1</sup>

<sup>1</sup> Meteorological Service of Canada, Canada

<sup>2</sup> Central Aerological Observatory, Russia

### SUMMARY

It is important to gain knowledge about the microphysical characteristics of continental clouds in order to properly understand their formation, their radiative properties and their ability to produce precipitation. Satellites to remote sensing of cloud properties, and cloud interactions with aircraft that fly through them require knowledge of cloud microphysics. Moreover, numerical simulations of global climate are sensitive to small systematic changes in cloud optical properties, but very few large data sets are available that document the characteristics of continental clouds. This paper summarizes  $9 \times 10^4$  km of in-cloud measurements made by the Central Aerological Observatory over the former USSR during 1977 to 1984. Statistical characteristics of total water content ( $W$ ), extinction coefficient ( $\beta$ ), effective diameter ( $D_{eff}$ ) and effective concentration ( $N_{eff}$ ) are summarized as functions of temperature and cloud type, for measurements archived at 700 m horizontal resolution. The effect of threshold sensitivity, or cloud definition, on the statistical distributions is discussed. Decreases of  $W$ ,  $\beta$ , and  $N_{eff}$  with colder temperatures are consistent with our general knowledge of cloud formation. For all temperature intervals and cloud types, correlations between pairs of  $W$ ,  $\beta$  and  $D_{eff}$  are too small thereby barring any hope of simple linear parameterizations. Differences in  $W$ ,  $\beta$ ,  $D_{eff}$  and  $N_{eff}$  for the various cloud types indicate changes in cloud formation mechanisms. These data can assist in verification studies of cloud parameterization schemes in GCMs, NWP models, and cloud-resolving models. The problems of cloud type, scale averaging, variability over a model grid cell, distribution of water between liquid and ice phases, and lumping together of precipitating and non-precipitating clouds must be considered in these studies.

KEYWORDS: Effective radius, extinction coefficient, total water content

### 1. INTRODUCTION

Statistical characteristics of cloud microphysical parameters such as water content, extinction coefficient, effective diameter and concentration of cloud particles are of great importance for climate studies, climate modelling, radar and satellite sensing, wave propagation etc. In-situ measurements and theoretical studies show that cloud microstructure depends on a number of different parameters such as cloud condensation nuclei (CCN) distribution, vertical velocities, turbulence, and entrainment (e.g. Pruppacher and Klett 1997). The ambient temperature  $T$  of saturated air and height of ascent of an air parcel define water vapor mass that can be converted into liquid. Therefore, cloud temperature is expected to be one of the main parameters governing cloud microstructure. Early studies by Lewis (1951) and Minervin (1954) showed the link between  $T$  and cloud water content. Later, this problem was studied in more detail by Borovikov and Mazin (1975), Mazin (1989, 1995), and Gultepe and Isaac (1997). There are limited studies of cloud particle concentration versus  $T$ . Thus, Korolev et al. (2000) and Gultepe et al. (2001) showed that the concentration of large particles ( $>125\mu\text{m}$ ) stays approximately constant within the range  $-30^\circ\text{C} < T < 0^\circ\text{C}$ . However, with the exception of Gultepe et al. (2001), there are few publications regarding the dependence of small particle concentration on  $T$ . Similarly, the temperature dependence of the extinction coefficient and the effective diameter of cloud particles are not well documented.

Simple visual observations show that different cloud types have different optical density. Some generate precipitation more frequently than others, while others do not produce precipitation at all. Therefore microphysical parameters should depend on cloud type as well. The statistical characteristics of water content for different cloud types were described by Mazin (1989) while extinction coefficient for various cloud types was studied by Kosarev et al. (1976) and Mazin et al. (1983).

It has been shown (e.g., Mitchell et al. 1995; Lohmann and Feichter 1997) that numerical simulations of global climate are sensitive to seemingly small, but systematic, changes to cloud optical properties. This is cause for great concern, particularly in light of the uncertainty surrounding indirect radiative forcing by anthropogenic aerosols (Lohmann and Feichter 1997). In the past, it was common to specify cloud microstructure, and

---

\* Corresponding author: Alexei Korolev, 28 Don Head Village Blvd., Richmond Hill, Ontario, L4C 7M6, Canada. E-mail: Alexei.Korolev@home.com

subsequent optical properties, based on observations (e.g., McFarlane et al. 1992). Procedures were, however, very simplistic: given  $T$ , assign the grid-cell mean water content (Feigelson 1978), fix droplet effective radius (Fouquart et al. 1990) and optical properties, and pass this information to plane-parallel radiative transfer algorithms (Stephens 1984). Understandably, the current trend is toward prognostic cloud water schemes (Sundqvist 1979; Tiedtke 1993) in which masses of condensed water obey conservation laws with various transformations and fluxes taken into consideration. Once the fractional area (or volume) of a grid-cell containing cloud is set (typically diagnostically), assumptions are made about droplet numbers and sizes, optical properties are computed using a parameterization such as Slingo's (1989), and again simple radiative transfer codes are employed.

It is known that for domains the size of GCM cells, cloud structure and optical properties typically vary greatly (e.g., Barker et al. 1996). Given the nonlinear relations between cloud processes (Pincus and Klein 2000), radiative transfer, and cloud optics, the climate modeling community is becoming increasingly aware of the importance of unresolved cloud structure. That is, simple mean values are likely not enough. The obvious next step is to include statistical descriptions of both unresolved cloud structure and radiative transfer. While suitable radiative transfer models are emerging (e.g., Oreopoulos and Barker 1999), little can be said about representation of unresolved cloud structure. While there is hope that satellite and cloud-resolving model data can help parameterize unresolved clouds, they are not free of significant limitations. For example, current satellites can retrieve only vertically-integrated (effective) measures of cloud microstructure or microstructure close to cloud tops. Cloud-resolving models, on the other hand, are to some extent parameterizations themselves and more often than not neglect microphysics. Though certainly not a panacea, aircraft observations can provide accurate, high spatial resolution *in situ* observations and should aid both large-scale models and cloud-resolving models (particularly those with explicit microphysical schemes such as Brenguier and Grabowski's (1993)).

In the early and mid 70s, the Laboratory of Cloud Physics (LCP) of Central Aerological Observatory (CAO) developed a set of aircraft probes for studying cloud microstructure. Included among these instruments were the Nevzorov hot-wire probe for measuring total water content (ice+liquid) and the Cloud Extinctionmeter for measuring the extinction of radiation within clouds and fogs. Both instruments were installed onboard the CAO Ilushin-18 and became the basis for the LCP Cloud Archive. The data set considered in the present study covers the period from 1977 to 1984 and includes about  $9.5 \times 10^4$  km of in-cloud measurements of cloud water content and extinction coefficient.

This paper presents a study of the statistical characteristics of total (ice+liquid) water content ( $W$ ), extinction coefficient ( $\beta$ ), effective diameter of cloud particles ( $D_{eff}$ ), and effective concentration ( $N_{eff}$ ) based on the LCP Cloud Archive. Both  $D_{eff}$  and  $N_{eff}$  were derived from measurements of  $W$  and  $\beta$  (Korolev et al. 1999a). Statistical characteristics of  $\beta$ ,  $W$ ,  $D_{eff}$ , and  $N_{eff}$  were examined as a function of  $T$  and cloud type. Cloud data were sorted into six  $10^\circ\text{C}$  temperature intervals between  $+10^\circ\text{C}$  and  $-50^\circ\text{C}$ , and into six groups associated with different cloud types. Classification by cloud type is discussed in Section 7. For each of the twelve groups, probability distributions and statistical parameters were calculated (Sections 5-8).

## 2. INSTRUMENTATION

Instruments aboard the CAO Ilushin-18 aircraft that are used to measure cloud microphysical and thermodynamical variables included: a cloud extinctionmeter (RP), a Nevzorov TWC probe (IVO), a cloud particle size spectrometer (AFSO) (20-120 $\mu\text{m}$ ), a precipitation particle size spectrometer (IRCh) (200-6000 $\mu\text{m}$ ), Particle Measurement System (PMS) particle size spectrometers FSSP-100 (2-47 $\mu\text{m}$ ), OAP-200X (10-320 $\mu\text{m}$ ), and OAP-2DC (25-800 $\mu\text{m}$ ), an up and down looking Doppler radar ( $\lambda = 3$  cm), a microwave radiometer ( $\lambda = 8$  mm), an up and down looking lidar, a dew point hygrometer; UV hygrometer; vertical and horizontal gust probes, a temperature fluctuation probe, and visible radiometers. These instruments were installed at different times and they participated in different flight projects. Even though data from all the probes were not included in the LCP archive, some excluded data were used to validate data in the archive. Results presented here are based on data from the Nevzorov TWC probe and the Cloud Extinctionmeter. A brief description of these instruments is given in the following two sections. Air temperature, true air speed, and air pressure used to interpret the collected data were measured with an accuracy of about  $\pm 1^\circ\text{C}$ ,  $\pm 2\%$ , and  $\pm 5\text{mb}$ , respectively. The true airspeed of the Ilushin-18 varied from  $100\text{ms}^{-1}$  below 2 km to  $160\text{ms}^{-1}$  above 7 km. Data were sampled at rates between 1Hz to 5Hz. One or two trained meteorologists, whose task was to observe and record the meteorological situation and to classify cloud types along the flight route, accompanied every flight.

(a). Measurements of Total Water Content

Total water content (ice+liquid) (TWC) was measured by the Nevzorov probe (Nevzorov 1980; Korolev et al. 1998) which is a constant temperature hot-wire probe similar in principle to the King probe (King et al. 1978). The Nevzorov probe has two distinct features. First, its sensor head consists of two wires: collector and reference. The collector sensor is exposed to the airflow and cloud particles. The reference sensor, being aerodynamically protected from collision with cloud particles, automatically compensates dry heat losses caused by fluctuations in air speed, air temperature, and pressure. This type of compensation makes it possible to improve the measurement accuracy relative to the King probe. The threshold sensitivity of the Nevzorov probe is estimated to be between 0.001 and 0.003 gm<sup>-3</sup> (Nevzorov 1980; Korolev et al. 1998). The second distinct feature of the Nevzorov probe is the conical hollow shape of the sensor. Such a sensor acts as a trap for both droplets and ice particles that impact with it. After capture by the sensor, ice particles are heated, melted and evaporated, whereas liquid droplets are just heated and evaporated. This makes it possible to measure total (ice + liquid) water content (TWC) of clouds. The concave shape of the Nevzorov TWC sensor also has an improved capability for precipitation size droplets (Korolev et al. 1998) as compared to the 1.6 mm diameter cylindrical King probe (Biter et al. 1987). For this paper, data associated with the liquid water sensor integrated with later versions of the Nevzorov probe were not available.

Total cloud water content was calculated as

$$W = \frac{V_{cd}^2}{SUL^*R_c} \quad (1)$$

where  $R_c$  is the resistance of the collector sensor;  $V_{cd}$  is the measured voltage across the collector sensor;  $S$  is the collector sample area;  $U$  is the air speed;  $L^*$  is the specific energy expended in heating and evaporating the water. For liquid cloud,  $L^*$  can be written as

$$L^* = C(T_e - T) + L(T_e) \quad (2)$$

where  $C_l$  is the specific heat of liquid water,  $T$  is an ambient air temperature, and  $L_l(T_e)$  is the latent heat of evaporation of water at temperature of evaporation  $T_e$ . In general, the temperature of evaporation  $T_e$  is less than the collector temperature  $T_c$ . The temperature  $T_e$  can be found from the mass balance equation (Nevzorov, 1983)

$$U\varepsilon W = \mu(E_s(T_e) - E_s(T)) \quad (3)$$

Here  $E_s(T)$  is the saturation vapour pressure at temperature  $T$ ,  $\mu$  is the mass transfer coefficient for the collector, and  $\varepsilon$  is the sensor collection efficiency. The evaporation temperature varies in the range  $T_c > T_e > T$ . For simplicity it is convenient to use an average value of  $L_l^* = 2580$  J/g, which adds a  $\pm 5\%$  error to estimates of LWC for the typical range of LWC for clouds with temperatures between  $-50^\circ\text{C}$  and  $+10^\circ\text{C}$  (Nevzorov 1983).

For ice particles

$$L_i^* = C_i(T_0 - T) + L_i + C_l(T_e - T_0) + L_l(T_e) \quad (4)$$

where  $C_i$  is the specific heat of ice,  $L_i$  is the latent heat of fusion, and  $T_0 = 0^\circ\text{C}$ . For most applications, the approximation  $L_i^* \approx 1.13L_l^*$  can be used in (2) and (4). Since for most cases the proportion between mass of ice and liquid particles captured by the sensor was unknown, the average value of expanded specific heat was assumed to be  $L^* = (L_i^* + L_l^*)/2$ . The error due to the uncertainty in the phase composition of a sample will be less than 7%.

Errors related to the estimation of the integral collision efficiency  $\varepsilon$  will be discussed in detail in Section 4.

(b). Measurements of Extinction Coefficient

Measurements of cloud transmittance in the visible were made with the Cloud Extinctionmeter (Nevzorov and Shugaev 1974; Kosarev et al. 1976; Korolev et al., 1999a). In essence, the Extinctionmeter measures the reduction of light intensity between an emitter and a receiver due to cloud. An incandescent tube lamp with a brightness temperature of about  $3000^\circ\text{C}$  is used as the source. A collimated light beam is directed at a cone-cube prism that reflects it back to the optical unit, where a receiving photodiode measures the intensity of transmitted light. The photodetector measures transmitted radiance for wavelengths between  $0.4\mu\text{m}$  and  $0.7\mu\text{m}$  with maximum sensitivity at  $0.59\mu\text{m}$ . Measured intensity is normalized by the intensity of the source with the background intensity of sunlight filtered out.

The optical unit of the Cloud Extinctionmeter was installed inside the fuselage of the Ilushin-18. The reflecting cone-cube prism was mounted on the aircraft's tail. The distance between the optical unit and the reflecting prism was  $L=7.8\text{m}$ , making the total distance between the source and photodetector  $15.6\text{m}$ . From Bouguer's law, the extinction coefficient was calculated as

$$\beta = -\frac{1}{2L} \ln \frac{F}{F_0} \quad (5)$$

where  $F$  and  $F_0$  are transmitted radiances for cloudy and clear air, respectively. The range of  $\beta$  was from  $1 \text{ km}^{-1}$  to  $250 \text{ km}^{-1}$ . As a frame of reference,  $\beta = 1 \text{ km}^{-1}$  corresponds to a monodispersion of  $10\mu\text{m}$  diameter droplets with a concentration and LWC of  $7 \text{ cm}^{-3}$  and  $0.004\text{gm}^{-3}$ , respectively. For  $100 \mu\text{m}$  diameter droplets, the concentration and LWC values are  $0.7\text{cm}^{-3}$  and  $0.04\text{gm}^{-3}$ , respectively.

Errors in the estimates of  $\beta$  are related mainly to forward-scattered radiation that enters the aperture of the detector (e.g., Deepak and Box 1978a,b). Errors and corrections to estimates of  $\beta$  are discussed in Section 4.

### (c). Description of data set

The majority of cloud microstructure measurements were made over different regions of Eastern Europe: Byelorussia, Estonia, Latvia, Lithuania, Russia, and Ukraine from 1977-1984. A few flights were carried out in Central Asia and Siberia. Data were collected during March, April, May, June, October, November, and December. Most data were measured during cold months: in October, November, December and March.

Measurements were made primarily in continental stratiform clouds associated with frontal systems. The total length of in-cloud flights is  $9.5 \times 10^4 \text{ km}$ . About 11% of all data were collected in stratus and stratocumulus clouds; 38% in altostratus and altocumulus clouds; 24% in nimbostratus; 19% in cirrus clouds; 4% in convective clouds; 0.3% in haze; and for  $\sim 4\%$  of the measurements, cloud type was not identified. Most data were collected during horizontal flight legs that varied from several kilometers to tens of kilometers.

Temperature measured within clouds varied from  $+10^\circ\text{C}$  to  $-55^\circ\text{C}$ . Figure 1 shows the length of in-cloud measurements versus altitude for different temperature intervals. Figure 2 shows in-cloud length versus temperature for different type of clouds. As seen from Table 1 and Figs. 1 and 2, the majority (92%) of clouds had temperatures below  $0^\circ\text{C}$ . Approximately 39% of the clouds were sampled in the temperature interval  $0^\circ\text{C}$  to  $-10^\circ\text{C}$ .

The flight level altitudes ranged from  $0.5 \text{ km}$  to  $10 \text{ km}$ . Figure 3 shows a scatter-diagram of cloud air temperature versus altitude and standard atmospheric temperature for mid latitudes for a winter season (McClatchey et al. 1972) indicated by solid line. As is seen from Figure 3, the average in-cloud temperature is close to that of the standard atmosphere. This makes it possible to convert the parameterization of cloud microstructure versus temperature into a dependence with altitude.

During processing, data were averaged over 5 second intervals, which corresponds to a distance of between  $0.55 \text{ km}$  and  $0.78 \text{ km}$  depending on altitude (Table 1). The total number of 5s average points is  $\sim 1.6 \times 10^5$ .

## 3. DATA PROCESSING

### (a). Calculation of effective diameter

The effective diameter (Hansen and Travis 1974) of a droplet size distribution  $f(D)$  is defined as

$$D_{\text{eff}} = \frac{\int_0^\infty f(D)D^3 dD}{\int_0^\infty f(D)D^2 dD} = \frac{\overline{D^3}}{\overline{D^2}} \quad (6)$$

Liquid water content  $W$  and extinction coefficient  $\beta$  are proportional to the third and second moments of  $f(D)$ , and expressed respectively as

$$W = \frac{\pi\rho_w}{6} \int_0^\infty f(D)D^3 dD \quad (7)$$

and

$$\beta = \frac{\pi}{4} \int_0^{\infty} Q(m, \lambda, D) f(D) D^2 dD, \quad (8)$$

where  $\rho_w$  is the liquid water density and  $Q$  is the extinction efficiency which is an oscillating function of  $\alpha = \pi D/\lambda$ , where  $\lambda$  is the wavelength of radiation, that asymptotes to 2 with increasing  $\alpha$  (van de Hulst 1957). For visible light, oscillations become small for  $D > 4 \mu\text{m}$ . Theoretical calculations and laboratory studies have shown that for non-spherical ice particles  $Q$  asymptotes to 2 regardless of shape and orientation (e.g., Volkovitsky et al. 1984; Shifrin 1988). For visible light, the oscillations of  $Q$  can be disregarded for ice particles with a characteristic size  $D > 10 \mu\text{m}$ . The effect of oscillations is also reduced for polychromatic light due to averaging over different  $\lambda$ . Thus, in this work  $Q=2$ . Therefore,  $D_{eff}$  can be expressed through  $W$  and  $\beta$  using (6), (7), and (8) as

$$D_{eff} = \frac{3}{\rho_w} \frac{W}{\beta} \quad (9)$$

which was used originally by Nevzorov and Shugaev (1972) and subsequently adopted by the radiative transfer community (e.g., Stephens 1978).

(b). *Effective concentration calculations*

The effective number concentration of droplets is defined as the concentration of the monodisperse size distribution having the same water content  $W$ , extinction coefficient  $\beta$  and effective diameter  $D_{eff}$  as a droplet size spectrum  $f(D)$ . As such,

$$W = \frac{\pi \rho_w}{6} N_{eff} D_{eff}^3 = \frac{\pi \rho_w}{6} \int_0^{\infty} f(D) D^3 dD \quad (10)$$

and

$$\beta = \frac{\pi Q}{4} N_{eff} D_{eff}^2 = \frac{\pi Q}{4} \int_0^{\infty} f(D) D^2 dD \quad (11)$$

Combining (10) and (11), and assuming that  $Q=2$ ,  $N_{eff}$  can be expressed as

$$N_{eff} = \frac{2 \rho_w^2 \beta^3}{9 \pi W^2} \quad (12)$$

Conversely, (10) and (11) yield another expression for  $N_{eff}$  of

$$N_{eff} = \frac{\left( \int_0^{\infty} f(D) D^2 dD \right)^3}{\left( \int_0^{\infty} f(D) D^3 dD \right)^2} = N_0 \left( \frac{D_2}{D_3} \right)^6 = N_0 \frac{D_3^3}{D_{eff}^3} = N_0 \frac{D_2^2}{D_{eff}^2} \quad (13)$$

where  $N_0 = \int_0^{\infty} f(D) dD$  is total number concentration,  $D_2$  and  $D_3$  are the mean area and mean volume diameters, respectively. Equation (13) indicates that the difference between  $N_0$  and  $N_{eff}$  decreases as the difference between  $D_2$  and  $D_3$  decreases. Since for any  $f(D)$ ,  $D_{eff} \geq D_3 \geq D_2$  is true, then  $N_0 \geq N_{eff}$  for all conditions. Only when  $f(D)$  is monodisperse does  $N_0 = N_{eff}$ .

(c). *Effective concentration calculations*

Corrections were applied to measured  $W$  and  $\beta$ . The fact that small cloud particles follow the airflow and may not impact on the sensor surface means that measured  $W$  are systematically low. They were corrected by a collision efficiency factor  $\varepsilon$  that depends on sensor shape, air speed, air pressure, temperature, as well as size, shape, and mass of cloud particles. For the Nevzorov sensor measured water contents  $W_{meas}$  were corrected (see Appendix for details) by

$$W = W_{meas} \frac{D_{eff, meas}^2 + a_2}{D_{eff, meas}^2 + a_1}, \quad (14)$$

where  $a_1$  and  $a_2$  are constants. Equation (14) is applied iteratively with calculations of retrieved  $D_{eff}$  as discussed in the previous section.

Estimation of  $\varepsilon$  for ice particles is complicated by their wide variety of shapes. *In-situ* measurements of ice particle habits (e.g. Korolev et al., 1999b) conducted by the Cloud Physics Research Division of Meteorological Service of Canada (MSC), with the help of a high-resolution imaging probe CPI (Lawson et al. 1998), showed that the majority of small ice particles ( $D < 40\mu\text{m}$ ), in all temperature intervals, were compact quasi-spheres. Since the bulk density of ice is only ten percent less than that of liquid, (14) can be applied to small ice particles. For larger ice particles corrections for  $\varepsilon$  become insignificant due to their large mass.

Measured  $\beta$  must be corrected because in scattering media the detector receives not only unattenuated photons, but photons that have been scattered as well. Since the optical thickness between the source and receiver is always small, and cloud particles are weak backscatters, the majority of scattered photons detected by the sensor undergo a single, near-forward, scattering event with a scattering angle less than the sensor's view cone  $\theta$  (e.g. Gumprecht and Sliepevich, 1953; Deepak and Box 1978a,b). If Bouguer's law were to be applied to the measured transmittances, the inferred  $\beta$  would be too small. The correction applied to  $\beta$  (see Appendix for details) was

$$\beta = \frac{2\beta_{meas}}{1 + e^{b_1 D_{eff, meas}^2 + b_2 D_{eff, meas}}}, \quad (15)$$

where  $b_1$  and  $b_2$  are constants. As with (14), (15) is applied iteratively with calculations of retrieved  $D_{eff}$  as discussed in the previous section.

Equations (14) and (15) give the first iterations of retrieved water content  $W_1$  and extinction coefficient  $\beta_1$  which when substituted into (9) and (12) yield the first iterations of corrected effective diameter  $D_{eff,1}$  and effective concentration  $N_{eff,1}$ . The second iterations of (14) and (15) used measured  $W_{meas}$ ,  $\beta_{meas}$ , and  $D_{eff,1}$ . Substituting  $W_2$  and  $\beta_2$  in (9) and (12) give the second iteration values  $D_{eff,2}$  and  $N_{eff,2}$ . These iterative mappings are applied until convergence conditions are satisfied.

The iterative process converges quickly. Figure 4 shows relative errors for measured values and the first four iterations of  $W_i$ ,  $\beta_i$ ,  $D_{eff,i}$ , and  $N_{eff,i}$  versus actual  $D_{eff}$ . As subsequent iterations have little effect, the number of iterations was limited to four in this study. The calculations shown in Fig. 3 were made for droplet size spectra described by a gamma distribution,  $f(D) = AD^a e^{-D/b}$ , whose modal diameter is  $D_{mod} = ab$ . The remarkable property of the suggested retrieval procedure is that the final errors for retrieved  $W_i$ ,  $\beta_i$ ,  $D_{eff,i}$ , and  $N_{eff,i}$  are weak functions of the shape of the distribution. For example, differences between relative errors of  $W_i$ ,  $\beta_i$ ,  $D_{eff,i}$ , and  $N_{eff,i}$  calculated for  $D_{mod}=2\mu\text{m}$  and  $D_{mod}=20\mu\text{m}$  do not exceed 3% for  $0.01 < b < 4$  which encompasses most observations. This retrieval method was applied to different type of size spectra (e.g. uniform, normal, distributions with negative and positive skewness), however the final error was approximately the same as in Fig. 4. The fact that the corrections are almost independent of size distribution shape implies that the suggested corrections can be applied to the majority of cases.

(d). Accuracy of estimation of  $W$ ,  $\beta$ ,  $D_{eff}$  and  $N_{eff}$

Figure 4 documents the performance of the iterative procedure described above when four iterations are applied. As seen from Fig. 4a, the maximum error for  $W$  after four iterations is only about 2-3%. Likewise, the maximum error for  $\beta$  is about 12% at  $D_{eff} \approx 80\mu\text{m}$  (Fig 4b) while for  $D_{eff} < 50\mu\text{m}$  the relative error does not exceed 3%. If the correction for forward scattering was not applied, the inferred  $\beta$  would be too small by 50% for  $D_{eff} > 200\mu\text{m}$  (precipitation case).

Figure 4c shows that the maximum relative error for retrieved  $D_{eff}$  is about 12% for  $D_{eff} \approx 80\mu\text{m}$ . For  $D_{eff} < 50\mu\text{m}$  relative errors for the retrieved  $\beta$  do not exceed 3%. If the corrections were not applied for  $D_{eff} > 200\mu\text{m}$ , the inferred effective diameters would be about two times larger. The maximum relative errors for retrieved  $N_{eff}$  are about 50% at  $D_{eff} \approx 80\mu\text{m}$  (Fig 4d). For  $D_{eff} < 50\mu\text{m}$  the relative errors in  $N_{eff}$  do not exceed 5%. Errors in the calculation of  $N_{eff}$  are most sensitive to errors in measurements of  $W$  and  $\beta$ . Thus, in the following discussion, it

is shown that the effective concentration should be considered only as an estimate of  $N_{eff}$ ; especially when  $W$  and  $\beta$  are small for then relative measurement errors are large.

It is worth mentioning that corrections for collision efficiency and forward scattering are systematic and that high-order iterations asymptotically approach curves that resemble the fourth iteration for  $W$ ,  $\beta$ ,  $D_{eff}$ , and  $N_{eff}$  as shown in Fig. 4 (see Section 4c). Taking into account that the relative errors of the asymptotic solutions to a first approximation are independent on the shape of the gamma-distribution, the resulting errors could be subjected to the following corrections. However, due to uncertainties related to other sources of errors, further corrections were disregarded in this study.

Regardless, the accuracy of  $D_{eff}$  and  $N_{eff}$  due to errors in measurements of  $W$  and  $\beta$  can be evaluated as follows. Differentiating the logarithm of (9) yields a relative accuracy of effective diameter  $\Delta D_{eff} = \Delta_W - \Delta_\beta$ , where  $\Delta_W$  and  $\Delta_\beta$  are relative errors in measurements of  $W$  and  $\beta$ , respectively. For 10% errors in  $\Delta_W$  and  $\Delta_\beta$ , the resulting error in  $D_{eff}$  ranges from 0% to 20% depending on the signs of  $\Delta_W$  and  $\Delta_\beta$ .

Similarly, the relative accuracy in measurements of effective concentration can be estimated from (12) as  $\Delta N_{eff} = 3\Delta_\beta - 2\Delta_W$ . For 10% errors in measurements of  $\Delta_W$  and  $\Delta_\beta$ , the resulting error in  $N_{eff}$  may range from 10% to 50% depending on the sign of the errors. Errors in the calculation of  $N_{eff}$  are most sensitive to errors in measurements of  $W$  and  $\beta$ . For this reason,  $N_{eff}$  should be considered only as an estimate of the effective concentration.

#### 4. STATISTICAL CHARACTERISTICS OF $W$ , $\beta$ , $D_{EFF}$ , AND $N_{EFF}$ IN DIFFERENT TEMPERATURE INTERVALS

Frequencies of occurrence of  $W$ ,  $\beta$ ,  $D_{eff}$ , and  $N_{eff}$  were calculated for 10°C intervals of temperature ranging from +10°C to -50°C.

Figure 5a shows the cumulative probabilities of  $W$ , in six temperature intervals. It shows that  $W$  decreases monotonically with decreasing  $T$  with the median of  $W$  decreasing from 0.16 gm<sup>-3</sup> at +10°C <  $T$  < 0°C to ~0.007 gm<sup>-3</sup> at -50°C <  $T$  < -40°C (Table 2). The maximum registered  $W$  averaged over the distance of about 0.6 km was 2.8 gm<sup>-3</sup>.

Figure 5b shows the cumulative probability distributions of  $\beta$  for different temperature intervals. It is seen that  $\beta$  gradually decreases with  $T$  such that the median of  $\beta$  decreases from 31 km<sup>-1</sup> at 0°C <  $T$  < +10°C to ~1.5 km<sup>-1</sup> at -50°C <  $T$  < -40°C (Table 2). The maximum measured  $\beta$  was about 320 km<sup>-1</sup>.

Figure 5c shows the cumulative probability distributions of  $D_{eff}$  for different temperature intervals.  $D_{eff}$  does not increase with  $T$  as distinctly as does  $W$  and  $\beta$ . Table 2 shows that median values of  $D_{eff}$  first increase with decreasing  $T$  to a maximum of 23 µm at -20°C <  $T$  < -10°C and then decrease for lower temperatures. The frequency distributions in Fig. 6 show that modal values of  $D_{eff}$ , for different temperature intervals, group in a relatively narrow size range between 9 µm and 16 µm. Figures 5c and 6 indicate a weak dependence of  $D_{eff}$  on  $T$ . It is interesting to note that the density distribution of  $D_{eff}$  for -50°C <  $T$  < -40°C is bimodal.

Figure 5d shows the cumulative probability distributions of  $N_{eff}$ . As  $T$  decreases from +10°C to about -20°C,  $N_{eff}$  decreases and then stays approximately constant down to -50°C (Table 2). Median values of  $N_{eff}$  at -50°C <  $T$  < +10°C vary from about 4 cm<sup>-3</sup> to 80 cm<sup>-3</sup>.

#### 5. RELATIONS BETWEEN $W$ , $\beta$ , $D_{EFF}$ , $N_{EFF}$ IN DIFFERENT TEMPERATURE INTERVALS

##### (a). Correlation between $W$ and $\beta$

Figure 7 shows a plot of  $W$  versus  $\beta$ . Contour lines indicate the isopleths of probability for finding  $W$  and  $\beta$  inside the contour. The average correlation coefficients  $K_{\beta W}$  for each temperature interval are shown in Table 3. As seen from Table 3, values of  $K_{\beta W}$  are rather low and vary between 0.55 and 0.69. Such low values indicate an absence, on average, of a clear relation between  $W$  and  $\beta$ . There is no statistically significant trend in  $K_{\beta W}$  with a change in  $T$ .

The scattering of  $W$  and  $\beta$  for the temperature intervals between -30°C <  $T$  < -10°C have two distinct lines around which the points are grouped. In Fig 7b,c,d these lines are marked by 1 and 2. The slope of these lines is defined by the ratio  $W/\beta$ , which in turn defines  $D_{eff}$  (Eq. 9). Therefore line 1 is mainly associated with smaller  $D_{eff}$  than line 2. This is in agreement with the shape of the frequency density distributions  $p(D_{eff})$  at temperatures -10°C <  $T$  < 0°C, -20°C <  $T$  < -10°C, -30°C <  $T$  < -20°C shown in Fig.6. As seen in Fig.6, the mentioned distributions have a second mode between 40µm and 60µm. The origin of this mode is possibly related to the

presence of precipitation, which would bias  $D_{eff}$  towards larger values. It is worth noting that at temperatures  $0^{\circ}\text{C} < T < +10^{\circ}\text{C}$ ,  $-50^{\circ}\text{C} < T < -30^{\circ}\text{C}$ , the effect of precipitation on the scatter of  $W$  and  $\beta$ , or the shape of  $p(D_{eff})$ , is significantly less than at  $-30^{\circ}\text{C} < T < 0^{\circ}\text{C}$ .

(b). Correlation between  $W$  and  $D_{eff}$

The scatter of  $D_{eff}$  versus  $W$  is shown in Figure 8. The correlation between  $D_{eff}$  and  $W$  was found to be rather high at cold temperatures ( $T < -20^{\circ}\text{C}$ ). As seen in Table 3,  $K_{WD}$  at  $-50^{\circ}\text{C} < T < -30^{\circ}\text{C}$  varies from 0.8 to 0.85. In general,  $K_{WD}$  increases monotonically with decreasing  $T$  from 0.23 at  $0^{\circ}\text{C} < T < +10^{\circ}\text{C}$  to 0.85 at  $-50^{\circ}\text{C} < T < -40^{\circ}\text{C}$  (Table 3). At  $-20^{\circ}\text{C} < T < 0^{\circ}\text{C}$  (Figs. 7b,c), the data are concentrated mainly around two distinct lines similar to the scatter of  $W$  and  $\beta$  as described in the previous section.

(c). Correlation between  $\beta$  and  $D_{eff}$

Figure 9 shows the scatter of  $D_{eff}$  versus  $\beta$ . The correlation coefficient between  $D_{eff}$  and  $\beta$  has a tendency to increase with decreasing  $T$  (Table 3). For all temperature intervals, however, the absolute value of  $K_{\beta D}$  is close to zero indicating an absence of a linear relation between  $D_{eff}$  and  $\beta$ . At  $-30^{\circ}\text{C} < T < +10^{\circ}\text{C}$ ,  $K_{\beta D}$  even goes negative.

## 6. STATISTICAL CHARACTERISTICS OF $W$ , $\beta$ , $D_{EFF}$ , AND $N_{EFF}$ FOR DIFFERENT CLOUD TYPES

The data were sorted by cloud type as determined by a trained, onboard, meteorologist. Based on the meteorologist's notes, a detailed vertical cross section of clouds was compiled for each flight. Cloud classification was based on the WMO definitions as described in the *Manual on the Observation of Clouds and Other Meteors (1975)* and the *International Cloud Atlas (1956)*. The classification of the characteristic forms of clouds included in the archive has been established in terms of "genera" (main group, e.g. *stratus*, *altocumulus*, *cirrus*), "species" (subdivision of genera, e.g. *lenticularis*, *congestus*, *uncinus*), and "variety" (special characteristics, e.g. *opacus*, *vertebratus*). Following the WMO definitions, cloud classification was based on cloud top and base altitudes and a visual evaluation of the appearance of cloud surfaces. The appearance of cloud top and base depends the distance from the observer, the solar zenith angle and the direction of observation. Clouds aloft that diffuse and shade the sun may also affect the appearance of a cloud's surface. These factors may bring subjective elements into the cloud classification. This problem mainly refers to discrimination between stratus (*St*) and stratocumulus (*Sc*) or altostratus (*As*) and altocumulus (*Ac*). Cloud classification from an aircraft is also hampered by rapidly changing environments, since the time for making a decision about cloud type is limited.

In cases when cloud top or base, or both, were unknown, cloud type was determined based on flight cross sections compiled by the onboard meteorologist. In approximately 4% of all cases, the clouds were not classified.

Cloud layers located in two "étages" simultaneously were classified as double genera (e.g., *Cs-As*, *As-Ns*, *St-Ns*). For example, if the upper part of a cloud was classified as *Cs* (i.e., upper level cloud) while the lower part was classified as *As* (middle level cloud), the whole cloud was be classified as *Cs-As*. The order of the genus in the double-named cloud was defined by the cloud type where the flight was conducted.

To minimize the ambiguity in cloud genus classification, clouds were grouped as follows:

- 1) Stratus and stratocumulus (*St, Sc*). This category included clouds in the altitude range from the Earth's surface to 2 km: *St*, *Sc*, *St-Sc*, *St-Ns*, *Sc-Ns*. The categories *St-Ns* and *Sc-Ns* have been defined as *St* or *Sc* layers seeded by precipitation from the above *Ns* layer.
- 2) Altostratus and altocumulus (*As, Ac*). These type of clouds include the layers *As*, *Ac*, *As-Ac*, *As-Ns*, *As-Cs* located between 2 km and 4 km
- 3) Nimbostratus (*Ns*) includes precipitating clouds *Ns*, *Ns-As*, *Ns-Cs* between 2 km and 6 km.
- 4) Cumulus (*Cu*) includes *Cu med*, *Cu cong*, *Cb*, *Cu emb*. The majority of clouds in this group were classified as embedded convection (*Cu emb*). Embedded convection was defined as zones with strong turbulence inside clouds associated with a frontal system.
- 5) Cirrus (*Ci*) included clouds classified as *Ci*, *Cs*, *Cc*, *Cs-Cc*, *Cs-As* located above 6 km.
- 6) "Haze" includes optically uniform regions with reduced visibility and without distinct boundaries. The altitude of these cloudy formations usually ranged between Earth's surface and 6 km.

Figure 10 shows cumulative probabilities of  $W$ ,  $\beta$ ,  $D_{eff}$ , and  $N_{eff}$  for the six cloud categories.

(a). Total water content

The convective clouds (mainly embedded convection regions) were found to have the highest  $W$  (Fig. 10a). The median  $W$  for convective clouds is about  $0.15 \text{ gm}^{-3}$  (Table 4) while for  $St, Sc$  it is approximately  $0.11 \text{ gm}^{-3}$  which is similar to that of  $Ns$ . The water content in  $As, Ac$  is less than in  $Ns$ . Cirrus clouds and hazes have the lowest  $W$ . The median value for  $Ci$  is  $\sim 0.01 \text{ gm}^{-3}$ .

(b). Extinction coefficient

$St, Sc$  were found to be the most optically dense clouds (Fig 10b). The median value of  $\beta$  for  $St, Sc$  is about  $30 \text{ km}^{-1}$ . The median value of  $\beta$  for embedded convective clouds is about  $25 \text{ km}^{-1}$ . Cirrus clouds and hazes are the most transparent clouds with the median value near  $2 \text{ km}^{-1}$ .

(c). Effective diameter

$St, Sc$  have, on average, smaller particles as compared to other clouds (Fig. 10c). The median  $D_{eff}$  for  $St, Sc$  is  $\sim 12 \text{ }\mu\text{m}$ . The cumulative distributions of  $D_{eff}$  for  $Cu, As, Ac, Ci, Ns$ , and haze group closely together (Fig. 10c). The density frequency distributions of  $D_{eff}$  shown in Fig. 11 indicate that modal values of the distributions for different cloud types change from about  $9 \text{ }\mu\text{m}$  to  $18 \text{ }\mu\text{m}$ . Nimbostratus clouds have the largest particles where approximately 10% of  $Ns$  have  $D_{eff} > 60 \text{ }\mu\text{m}$ . This is related to the presence of precipitation size particles, which enhance  $D_{eff}$ . It is encouraging to note that the average value of  $D_{eff}$  for  $St, Sc$  (i.e. low level non-precipitating clouds) is  $15.3 \text{ }\mu\text{m}$ , which agrees well with that of  $16.4 \text{ }\mu\text{m}$  obtained by Han et al.'s (1994) from ISCCP satellite estimates for the northern hemisphere.

(d). Effective concentration

Cumulative probabilities in Fig. 10d show that  $St, Sc$  have the highest concentrations. The median value of  $N_{eff}$  in  $St, Sc$  is  $\sim 145 \text{ cm}^{-3}$  (Table 4). The statistical characteristics of  $N_{eff}$  for  $Ns$  and  $As, Ac$  are close to each other. Cirrus clouds and haze have lowest effective concentration.

7. RELATION BETWEEN  $W$ ,  $\beta$ ,  $D_{EFF}$ , AND  $N_{EFF}$  FOR DIFFERENT CLOUD TYPES

(a). Correlation between  $W$  and  $\beta$

Figure 12 shows a scatterplot of  $W$  versus  $\beta$  for different cloud types. The correlation coefficients for different cloud types are shown in Table 5. Low-level stratiform clouds (Fig. 12a) were found to have a rather high correlation between  $W$  and  $\beta$ ; i.e.,  $K_{\beta W} = 0.75$  (Table 5). The highest values of  $K_{\beta W}$  are for hazes at 0.89. Nimbostratus and middle level clouds ( $As, Ac$ ) have values of 0.6 and 0.58, respectively. The decreased  $K_{\beta W}$  for  $Ns, As, Ac$  is likely caused by precipitation size particles. In convective zones, the effect of precipitation on  $K_{\beta W}$  is not that noticeable as in  $Ns, As, Ac$ . On average,  $K_{\beta W}$  is higher when the data are grouped by cloud types as compared to when the data are grouped by  $T$ . This bolsters confidence for the cloud classification.

(b). Correlation between  $W$  and  $D_{eff}$

Figure 13 shows a scatterplot of  $D_{eff}$  versus  $W$  for different cloud types. Low and middle level ( $St, Sc, Ns, As, Ac$ ) and convective ( $Cu$ ) clouds have two distinct lines around which points are concentrated (Fig 13 a,b,c,d). Such scattering of points results in rather low correlation coefficients. The values of  $K_{WD}$  in  $St, Sc, Ns, As, Ac, Cu$  varies from 0.22 to 0.48. For haze and cirrus clouds the  $D_{eff}-W$  points are grouped around one line (Table 5). As a result, values of  $K_{WD}$  in haze and cirrus clouds are rather high at 0.73 and 0.75, respectively.

(c). Correlation between  $\beta$  and  $D_{eff}$

Figure 14 shows a scatterplot of  $D_{eff}$  versus  $\beta$ . The correlation coefficient  $K_{\beta D}$  between  $D_{eff}$  and  $\beta$  is negative in all  $T$  intervals and close to zero (Table 5). Similar to the previous case, in low and middle level ( $St, Sc, Ns, As, Ac$ ) and convective ( $Cu$ ) clouds, points are concentrated around two distinct lines (Fig 14 a,b,c,d). In these clouds  $K_{\beta D}$  are negative and vary from  $-0.2$  to  $-0.3$ . In haze and cirrus clouds,  $K_{\beta D}$  is positive and equal to 0.47 and 0.17, respectively (Table 5).

## 8. DISCUSSION

### (a). *The effect of threshold sensitivity on statistical distributions*

The distributions of the microphysical parameters and its characteristic values are sensitive to the threshold values. For example, the median of a parameter will increase as the threshold increases. Threshold values are directly linked to the question: “what is a cloud?” The definition of cloud may vary depending on the type of research. Thus in radar studies, the threshold value for detection is defined by  $ND^6$ , so some clouds having relatively high  $W$  and  $\beta$  that are visible to the eye may go undetected by the radar. In lidar studies invisible objects with  $\beta \cong 0.1 \text{ km}^{-1}$  may be of interest. So different research groups using different instruments for cloud studies would be interested in different types of statistics of the same microphysical parameters. Mazin and Minervin (1993) have discussed this subject in some detail.

This study employed thresholds for the water content of  $W_{th} = 0.001 \text{ gm}^{-3}$  and  $\beta_{th} = 0.5 \text{ km}^{-1}$  for the extinction coefficient. Though errors in measurement of such low  $W$  and  $\beta$  may be relatively large, this does not affect noticeably the associated cumulative distributions. Increasing  $W_{th}$  from  $0.001 \text{ gm}^{-3}$  to  $0.005 \text{ gm}^{-3}$  increases the median by 20% at  $0^\circ\text{C} < T < +10^\circ\text{C}$ , about 200% at  $-10^\circ\text{C} < T < -20^\circ\text{C}$ , and 360% at  $-50^\circ\text{C} < T < -40^\circ\text{C}$ . Approximately the same increase in the median of  $\beta$  occurs when  $\beta_{th}$  is increased from  $\beta = 0.5 \text{ km}^{-1}$  to  $\beta = 2.5 \text{ km}^{-1}$ . As seen from the above example, transparent and low water content clouds at low temperatures are more sensitive to changes in threshold parameters. It is also worth noting that lower percentile values (e.g., 5%) are considerably more sensitive to changes in threshold than are higher percentile values (e.g., 95%).

As discussed in Section 4d,  $D_{eff}$  and  $N_{eff}$  are sensitive to errors in measurements of  $W$  and  $\beta$ . To avoid large errors,  $W_{th}$  and  $\beta_{th}$  were increased to  $0.003 \text{ gm}^{-3}$  and  $2 \text{ km}^{-1}$ , respectively, for the calculation of  $D_{eff}$  and  $N_{eff}$ . For smaller  $W_{th}$  and  $\beta_{th}$ , relative errors in measurements of  $W$  and  $\beta$  may reach 50% or more. As a consequence, errors in  $D_{eff}$  and  $N_{eff}$  will be even higher. Increasing the thresholds  $W_{th}$  and  $\beta_{th}$  resulted in a considerable converging of the distributions of  $D_{eff}$ . Figure 15 shows the frequency probability distributions  $p(D_{eff})$  calculated for  $W_{th} = 0.005 \text{ gm}^{-3}$  and  $\beta_{th} = 5 \text{ km}^{-1}$ . Increasing  $W_{th}$  and  $\beta_{th}$  much more does not change significantly the shape of distributions  $p(D_{eff})$  as compared to that shown in Fig. 15. This results in the finding that clouds with  $W > 0.005 \text{ gm}^{-3}$  and  $\beta > 5 \text{ km}^{-1}$  have the same frequency distributions of  $D_{eff}$ . This may have tremendous importance for GCMs.

### (b). *Comparisons with previous results*

Mazin (1995) studied probability distributions of  $W$  versus  $T$  for the same data set as used in the present work. Basically, characteristic values of  $W$  obtained in the present study are larger than in Mazin (1995). For example, the median  $W$  obtained in this study is 10% to 40% larger. The reason for this is two-fold. First, Mazin (1995) had included samples with zero  $W$ ; i.e.  $W_{th} = 0$ . Such points were assumed to describe intracloud holes. However, recalling that the sampling interval is  $\sim 0.54 - 0.77 \text{ km}$  (Table 1), samples with zero  $W$  likely represent intercloud space rather than intracloud holes. For this reason, such samples were excluded from the present statistics. The second reason is that Mazin (1995) did not apply corrections based on collection efficiency. Such corrections increase characteristic values of  $W$ .

Probability distributions of LWC as a function of  $T$  measured by the King probe were investigated by Gultepe and Isaac (1997) for measurements made in North America. The median LWC obtained in their study is higher for low  $T$  and lower for high  $T$ . This confusion may be explained by the higher threshold sensitivity of the King probe ( $0.02 \text{ gm}^{-3}$ ). The second reason is that the King probe measures mainly liquid water content which is systematically less than  $W$  studied in this paper.

Comparisons between median  $\beta$  obtained for different cloud types in Mazin et al. (1983) show reasonably good agreement with those found in the present study.

### (c). *Dependence of $W$ , $\beta$ , $D_{eff}$ and $N_{eff}$ on ambient temperature*

The decrease of  $W$ ,  $\beta$ , and  $N_{eff}$  with a decrease of ambient  $T$  is in agreement with general knowledge of cloud formation. The decrease in  $T$  would result in a decrease of water content that could condense during an ascent. Since ascent of cloud parcels is limited by the depth of a cloud layer, which in the case of stratiform cloud usually varies from 100 m to about 1 km, one can expect *on average* a decrease in water content with a decrease in  $T$ . This explains the observed lowering of  $W$  with decreasing  $T$ . Here the effects of altitude of ascent, entrainment and mixing, and sedimentation of precipitation were not considered. These effects in each specific

case may destroy the above argument. However, the bottom line presented in study is that for stratiform cloud,  $W$  is, on average, a function of ambient temperature.

Activation of cloud droplets is governed by the velocity of vertical ascent and CCN distribution. Vertical velocity defines maximum supersaturation, which together with CCN distribution defines the number concentration of activated droplets. Since convective activity and CCN concentration decrease on average with colder temperatures (higher altitudes), the number concentration of droplets is expected to decrease with  $T$  as well. As seen from Fig. 5d  $N_{eff}$  decreases as  $T$  decreases from  $+10^{\circ}\text{C}$  to  $-30^{\circ}\text{C}$ . For temperatures between  $-30^{\circ}\text{C}$  and  $-50^{\circ}\text{C}$ ,  $N_{eff}$  does not change noticeably and it stays approximately constant. For  $T < -30^{\circ}\text{C}$ , most cloud particles are expected to be ice. Therefore  $N_{eff}$  at temperatures below  $-30^{\circ}\text{C}$  may be considered as a concentration of ice particles. The constant concentration of ice at  $-50^{\circ}\text{C} < T < -30^{\circ}\text{C}$  is an interesting phenomenon that requires further explanation.

The condensed cloud water and the particle number concentration may be considered as the primary microphysical parameters that are governed by thermodynamical processes in clouds. To a first approximation, the formation of condensed water and number concentration occurs independent of each other. Therefore, the behavior of  $\beta$  versus  $T$  can be considered as a result of changes to both  $W$  and  $N_{eff}$ .

The independence of the distribution of  $D_{eff}$  on  $T$  is a remarkable phenomenon that can only be explained with further experimental and theoretical studies.

*(d). Dependence of  $W$ ,  $\beta$ ,  $D_{eff}$  and  $N_{eff}$  on altitude*

Figure 3 indicates that for the present dataset,  $T$  is, on average, a function of altitude. The dependence of  $T$  on  $H$  can be well approximated by the standard atmosphere for mid latitudes for a winter season (solid line in Fig. 3) (McClatchey et al. 1972). This allows one to use the standard atmosphere for the parameterization of  $W$ ,  $\beta$ ,  $D_{eff}$  and  $N_{eff}$  as a function of  $H$ , which may be useful for GCMs and other applications.

*(e). Correlation between  $W$ ,  $\beta$  and  $D_{eff}$*

Diagrams in Figs 7 and 12 show a large scattering of  $W$  and  $\beta$  points. The data presented in Tables 3 and 5 indicate that on average for all temperature intervals and all cloud types (probably excluding haze and low-level stratiform clouds) the correlation coefficient between  $W$  and  $\beta$  is too low to allow any linear parameterization. However, for individual clouds or subsections of a cloud, the correlation coefficient  $K_{\beta W}$  exceeds 0.8 in approximately 65% of all cases. Figure 16 demonstrates the frequency of occurrence of  $K_{\beta W}$  for the whole data set where  $K_{\beta W}$  was calculated for each cloud leg presented in the archive as a separate record. The length of cloud records varied from a few kilometers to tens of kilometers. The following two examples demonstrate two extreme cases in the correlative behavior of  $W$  and  $\beta$ . Figure 17 shows time histories of  $W$ ,  $\beta$ ,  $D_{eff}$  and  $N_{eff}$  for the case of high correlation between  $W$  and  $\beta$  ( $K_{\beta W} = 0.98$ ). It is interesting to note that  $N_{eff}$  does not correlate with any other parameter. Another case shows low correlation between  $W$  and  $\beta$  with  $K_{\beta W} = -0.02$ . It is seen from Fig. 18 that  $D_{eff}$  correlates better with  $W$  than with  $\beta$ . The analysis of  $K_{\beta W}$  shows that in approximately 3% of all cases  $K_{\beta W}$  is negative. There are few cases when  $K_{\beta W} < -0.9$ .

The fact that individual clouds often have  $K_{\beta W} > 0.8$  (Fig. 16) but the ensemble values of  $K_{\beta W}$  are typically between 0.5 and 0.7 (Figs 7 and 12) has a simple explanation. The high correlation between  $W$  and  $\beta$  in a particular cloud indicates that the ratio  $W/\beta$ , which characterizes  $D_{eff}$ , stays approximately constant. However, the ratio  $W/\beta$  or  $D_{eff}$  varies from cloud to cloud. This means that in a  $W$ - $\beta$  diagram, points for different clouds will be grouped along different directions, resulting in a large scatter for the entire population of cloudy situations.

*(f). Effective concentration*

As was mentioned in Section 4b,  $N_0 \geq N_{eff}$  for all conditions. Therefore  $N_{eff}$  may be used as an estimate of the lower limit of the particle number concentration  $N_0$ . The difference between  $N_0$  and  $N_{eff}$  reflects the shape of the droplet size distribution. Equation (13) shows that the larger the ratio  $N_0/N_{eff}$ , the larger will be the value  $(D_3/D_2)^6$ , which increases with increasing concentration of large droplets. For liquid low-level stratiform clouds,  $(D_3/D_2)^6$  may vary from 1.5 to 2.5 (Korolev et al. 1999a). For mixed and ice clouds,  $(D_3/D_2)^6$  may vary over a wider range.

The effective concentration may play an important role in parameterization of clouds since four parameters of droplet size distribution  $W$ ,  $\varepsilon$ ,  $D_{eff}$ , and  $N_{eff}$  form a system of parameters where any two parameters define the remaining two. In simple terms, an arbitrary droplet size distribution is replaced by a monodisperse size spectrum with the same  $W$ ,  $\varepsilon$ , and  $D_{eff}$  but new concentration  $N_{eff}$ . The four variables  $W$ ,  $\beta$ ,  $D_{eff}$ , and  $N_{eff}$  may form a system of parameters well suited for modeling cloud radiative processes. The introduction of  $N_{eff}$  allows for model calculations of the effect of droplet number concentration while maintaining a self-consistent system of variables.

Some researchers assume, for the parameterization of cloud microstructure, that

$$D_{eff} = \left( \frac{6W}{\pi\rho KN_0} \right)^{1/3} \quad (16)$$

where  $K$  is a coefficient that varies from 1 to 1.6 (e.g., Fouquart et al. 1990; Bower and Choulaton 1992; Martin et al. 1994). In fact, (12) and (13) yield

$$K = \left( \frac{D_2}{D_3} \right)^6 = \left( \frac{D_3}{D_{eff}} \right)^3 = \left( \frac{D_2}{D_{eff}} \right)^2. \quad (17)$$

The spatial variations of  $(D_2/D_3)^6$  measured in real clouds indicate that the coefficient  $K$  may vary by tens of percent from its average value in the same cloud (Korolev et al. 1999a; Wood 2000).

#### (g). *Applicability to GCMs*

These data may be useful for GCM and NWP studies through simple comparisons of mean values for given ranges of temperature or height. For example, if one were to sample, in a GCM,  $W$ ,  $\beta$ , and  $D_{eff}$  for continental stratiform clouds and compute simple mean values for ranges of  $T$ , they could be compared to values in Table 2. However, the mean values are dependent on the scale being considered. Gulpepe and Isaac (1999) showed how cloud parameters can vary depending on the averaging interval. The scale value of 0.7 km was used in this study and it could not practically be extended to larger sizes due to limitations of the data set. This scale is reasonable for a mesoscale model, but not for a GCM.

Current GCMs and NWP models use prognostic schemes to predict cloud water mass and so parameterizations of mean  $W$  as a function of  $T$  are not required. What GCMs need are parameterizations of unresolved fluctuations in cloud density; mean values are necessary but not sufficient (e.g., Barker et al. 1999). Thus, one could envisage a scheme that goes something like:

- The GCM cloud scheme provides mass of condensed water and cloud volume;
- Based on other resolved variables (and cloud fraction perhaps), the unresolved distribution of  $W$  is diagnosed;
- Using this distribution of  $W$ , set distributions of  $\beta$  and  $D_{eff}$  based on conditional distributions similar to those shown here, and determine suitable cloud optical properties and radiative fluxes.

It is essential to note that distributions of  $W$  presented here are not commensurate with distributions of  $W$  needed by a GCM grid-cell. This is because the data presented here apply to  $\sim 700$  m horizontal resolution. It would be incorrect to assume that the GCM's grid-mean  $W$  can draw conditional distributions of  $\beta$  and  $D_{eff}$  from Figs. 5bc and 10bc to represent the distribution of these variables over a cell. Rather, a distribution of  $W$  should draw ensemble-average distributions of  $\beta$  and  $D_{eff}$ . Though it would be appropriate to create the kinds of distributions and correlations shown here for much longer transects, the integrity of the statistics decline rapidly as sample size diminishes.

An additional question rarely raised in the GCM radiation community, but that is inherent to the statistics presented here, is: should that portion of a grid-cell's cloud water diagnosed as precipitation be included in determination of optical properties? It is likely that much of the variability shown here is derived from mixing precipitation with cloud droplets; and there is no way to separate the relative contributions. As precipitation is almost invisible to solar and terrestrial radiation, its contribution to  $W$  (and suitably modulated  $\beta$  and  $D_{eff}$ ) is usually neglected in a GCM. If the data presented here, or similar data, were to be used to derive a parameterization, contributions from precipitation and cloud droplets must be known.

Two other factors must be considered. First, one should always be mindful of extrapolating optical property parameterizations based on data collected selectively in particular cloud types to all cloud types everywhere all

the time. Within GCMs or NWP models, schemes must be developed that track cloud types in greater detail than simply continental and maritime. Second, because of the particular data set, total water content was reported in this work. The ideal parameterization would, however, discriminate between ice and liquid phase.

*(h). Applicability to satellite missions*

The next generation of climate and weather research satellites will include active sensors such as cloud-profiling radars and lidars (e.g., CloudSat and Picasso-Cena scheduled for launch in 2003). These satellites will provide, for the first time, global information on the vertical structure of cloud. For most clouds, however, a significant amount of ambiguity will exist regarding the determination of  $W$  and  $D_{eff}$ . For example, a given radar reflectivity might derive from small  $W$  with few large droplets, or large  $W$  with many small droplets. One could envisage that data such as those presented here might aid in validation of inferred distributions of  $W$  and  $D_{eff}$ . In another respect, the relations presented here could be used to establish distributions of likely values of  $W$  and  $D_{eff}$  inferred from radar reflectivities.

*(i). Applicability to aircraft in-flight icing*

Aircraft must be designed to fly into supercooled cloud, or they must avoid those clouds in order to prevent problems associated with airframe and engine icing. De-icing or anti-icing systems must be engineered to withstand reasonable extremes in terms of cloud water or total water content, droplet size, and temperature. The aircraft design or certification envelopes (e.g. FAR 25, Appendix C; see Federal Aviation Administration, 1999) were developed before the advent of modern cloud physics instrumentation in the 1970s. This data set provides a useful summary from eastern Europe and Asia to enable another more recent comparison with the older design criteria. Further work will be needed to perform this comparison, but the median liquid water contents of  $0.1 \text{ g m}^{-3}$  for *St*, *Sc*, *Cu* and *Ns* near  $0$ – $-10$  °C are very similar to earlier and more recently measured values (e.g. Sand et al, 1984; Isaac, 1991; and Cober et al., 2001).

## 9. CONCLUSION

The following conclusions have been drawn from this study:

- Cumulative probability distributions for  $W$ ,  $\beta$ ,  $D_{eff}$ , and  $N_{eff}$  have been calculated for six  $10^\circ\text{C}$  temperature intervals in the range  $-50^\circ\text{C} < T < 0^\circ\text{C}$ . Total water content and extinction coefficient were found to decrease monotonically with decreasing temperatures. Characteristic values of effective diameter do not change much with temperature. To a first approximation,  $D_{eff}$  may be considered as a weak function of  $T$ . The effective concentration rapidly decreases with a decrease of temperature from  $+10^\circ\text{C}$  to  $-20^\circ\text{C}$ , and then remains approximately constant at temperatures  $-50^\circ\text{C} < T < -20^\circ\text{C}$ .
- Cumulative probability distributions for  $W$ ,  $\beta$ ,  $D_{eff}$  and  $N_{eff}$  have been calculated for six cloud categories: *St, Sc; Ns; As, Ac; Ci; Cu; haze*. Probability distributions of  $W$ ,  $\beta$ ,  $D_{eff}$  and  $N_{eff}$  have distinct features in each cloud category. Differences in  $W$ ,  $\beta$ ,  $D_{eff}$  and  $N_{eff}$  indicate different regimes for cloud microstructure formation in various cloud types.
- On average, correlation coefficients for the total population of  $W$  and  $\beta$  at all temperatures are low ( $K_{\beta W} \sim 0.55$ – $0.69$ ). However, in individual clouds or parts of clouds,  $K_{\beta W}$  can be high: in about 70% of the clouds,  $K_{\beta W}$  exceeds 0.8. The correlation between  $W$  and  $D_{eff}$  gradually increases as temperature decreases. At cold temperatures ( $-50^\circ\text{C} < T < -30^\circ\text{C}$ ),  $K_{WD}$  reaches about 0.8–0.85. There is no significant linear relation between  $\beta$  and  $D_{eff}$ .
- On average,  $K_{\beta W}$  in different cloud types varies from about 0.58 to 0.85.
- An analysis of the correlation between pairs of  $W$ ,  $\beta$ , and  $D_{eff}$  has shown that on average the correlative relations are rather low. This finding makes the use of parameterization of relations between  $W$ ,  $\beta$ , and  $D_{eff}$ , which are sometimes used in GCMs (e.g., McFarlane et al. 1992), rather questionable. The results of this study send a message to climate community to search for another approach to incorporate microphysical characteristics of clouds into climate models.
- The data presented in this work, if used carefully, can assist in verification studies of cloud parameterization schemes in GCMs and NWP models. The problems of cloud type, scale averaging, variability over the model grid, distribution of water between the liquid and ice phase, and lumping of precipitating and non-precipitating clouds must be considered in these verification studies.

APPENDIX

Corrections to measured water content and extinction coefficient

The purpose of this appendix is to present details of the corrections to the initial inferences of cloud water content  $W$  and extinction coefficient  $\beta$ .

(a). Water content

For liquid droplets, the collision efficiency  $\varepsilon$  was calculated for a rectangular plate having the same cross section as the Nevzorov probe (Mazin et al. 1996). The obtained dependence of the collision efficiency on droplet diameter  $D$  can be approximated for  $D > 1\mu\text{m}$  as

$$\varepsilon = \frac{D^2 + a_1}{D^2 + a_2}, \quad (\text{A1})$$

where  $a_1 \approx 15\mu\text{m}^2$  and  $a_2 \approx 50\mu\text{m}^2$ . Measured ( $W_{\text{meas}}$ ) and actual ( $W$ ) water content are related then as

$$W_{\text{meas}} = \frac{\pi\rho_w}{6} \int_0^\infty \varepsilon(D) f(D) D^3 dD = \varepsilon^* W \quad (\text{A2})$$

where  $\varepsilon^*$  is the integral collection efficiency defined as

$$\varepsilon^* = \frac{\int_0^\infty \varepsilon(D) f(D) D^3 dD}{\int_0^\infty f(D) D^3 dD} \quad (\text{A3})$$

Since particle size distributions were not measured,  $\varepsilon^*$  could not be calculated. To estimate the effect of the collision efficiency, the particle size distribution was assumed to be monodisperse with a particle size equal to the measured effective diameter  $D_{\text{eff meas}}$  derived from (9) using the measured water content  $W_{\text{meas}}$  and the extinction coefficient  $\beta_{\text{meas}}$ . Under this assumption substituting (9), (A1) and (A2) yields

$$W = \frac{W_{\text{meas}}}{\varepsilon(D_{\text{eff meas}})} = W_{\text{meas}} \frac{D_{\text{eff meas}}^2 + a_2}{D_{\text{eff meas}}^2 + a_1} \quad (\text{A4})$$

(b). Extinction coefficient

To derive the extinction coefficient, one measures the apparent  $\beta_{\text{meas}}$  related to the apparent scattering efficiency  $Q_{\text{meas}}$ , which is different from actual value  $Q$ . The scattering efficiency  $Q$  characterizes the light scattered in all directions and is equal to

$$Q = \frac{1}{\alpha^2} \int_0^\pi (i_1 + i_2) \sin \theta d\theta \quad (\text{A5})$$

where  $i_1$  and  $i_2$  are Mie intensity functions (e.g., van de Hulst, 1957). The apparent scattering efficiency  $Q_{\text{meas}}$  is defined as

$$Q_{\text{meas}} = \frac{1}{\alpha^2} \int_\theta^\theta (i_1 + i_2) \sin \theta d\theta \quad (\text{A6})$$

and characterizes the light scattered in all directions except within a cone of half-angle  $\theta$ . Thus using (A5) and (A6), the correction factor for the measured extinction coefficient is

$$G = \frac{Q_{\text{meas}}}{Q} = 1 - \frac{1}{\alpha^2 Q} \int_0^\theta (i_1 + i_2) \sin \theta' d\theta' \quad (\text{A7})$$

Calculations of  $G$  from (20) for small  $\theta$  shows that as the droplet size increases,  $G$  approaches 0.5 asymptotically (Deepak and Box 1978a). This is related to the diffraction nature of forward scattered photons. For large non-absorbing particles, approximately half of the scattered radiation arises through reflection and refraction, while the other half is determined by diffraction. Since diffraction is defined mainly by particle cross-

section, forward scattering for ice particles will be approximately the same as for spheres with the equivalent cross-section (e.g. Shifrin, 1988). Therefore, (20) can be used as a first order approximation for ice particles.

The correction factor  $G$  was calculated for the Cloud Extinctionmeter having  $\theta \approx 0.3^\circ$  (Nevzorov 1971; Kosarev et al. 1976). Changes of  $\theta$  along the beam, multiple scattering, and peculiarities of optical diagram of the probe were taken into account. The results can be parameterized to within about 2% by

$$G = \frac{1}{2} \left( 1 + e^{b_1 D^2 + b_2 D} \right) \quad (\text{A8})$$

where  $b_1 = -6.51 \cdot 10^{-4} \mu\text{m}^{-2}$ , and  $b_2 = 5.5 \cdot 10^{-3} \mu\text{m}^{-1}$ . For the Cloud Extinctionmeter,  $G$  reaches 0.5 for droplets with  $D \geq 80 \mu\text{m}$ . On average, for a typical cloud particle size spectrum having a gamma-distribution with modal diameter less than  $30 \mu\text{m}$ , the accuracy of the Cloud Extinctionmeter is estimated to be 12% (Kosarev et al. 1976). For precipitation cases, errors in measurement of  $\beta$  may reach 50%.

The measured and actual  $\beta$  are related as

$$\beta_{meas} = \frac{\pi}{4} \int_0^\infty G(D) Q(D, \lambda, m) f(D) D^2 dD = G^* \beta \quad (\text{A9})$$

where  $G^*$  is defined as

$$G^* = \frac{\int_0^\infty G(D) Q(D, \lambda, m) f(D) D^2 dD}{\int_0^\infty Q(D, \lambda, m) f(D) D^2 dD} \quad (\text{A10})$$

Since the particle size distributions were unknown,  $G$  was estimated based on measured effective diameter  $D_{eff\ meas}$ . Combining (A8) and (A9) yields

$$\beta = \frac{\beta_{meas}}{G(D_{eff\ meas})} = \frac{2\beta_{meas}}{1 + e^{b_1 D_{eff\ meas}^2 + b_2 D_{eff\ meas}}} \quad (\text{A11})$$

#### ACKNOWLEDGEMENTS

The present paper is based on measurements made by the Cloud Physics Laboratory of the Central Aerological Observatory (CAO) (Moscow). The authors are grateful to Dr. Anatoly Nevzorov, designer of the aircraft cloud instrumentation, whose role in the production of this paper is hard to overestimate. We also appreciate his valuable comments and discussion of this work. The authors appreciate our colleagues V. Shugaev and A. Kosarev who participated in data collection and data processing. Special thanks to A. Ataman, S. Burkovskaya, E. Ivanova, and N. Monakhova of CAO for the initial data processing and archiving. We would also like to thank Paul Lawson of SPEC for his interest and encouragement in performing this work through support by NASA SBIR Contract No. NAS5-98032, which funded delivery of the CAO data to SPEC. Many thanks to Robert Wood of University of Washington for his useful comments. Alexei Korolev has performed this work under the contract KM173-0-2062 to the Meteorological Service of Canada. Partial funding for the present study was obtained from the National Search and Rescue Secretariat of Canada and the Canadian Panel on Energy Research and Development.

#### REFERENCES

- Barker, H. W., Wielicki, B. A. and Parker, L. 1996 A Parameterization for Computing Grid-Averaged Solar Fluxes for Inhomogeneous Marine Boundary Layer Clouds. Part I: Validation using satellite data. *J. Atmos. Sci.*, **53**, 2304-2316
- Barker, H. W., G. L. Stephens, and Q. Fu, 1999: The sensitivity of domain-averaged solar fluxes to assumptions about cloud geometry. *Q. J. R. Meteorol. Soc.*, **125**, 2127-2152.
- Biter C. J., Dye, J. E., Huffman, D. and King, W. D. 1987 The drop response of the CSIRO liquid water content. *J. Atmos. Ocean Techn.*, **4**, 359-367
- Bower, K. N. and Choullarton, T. W. 1992 A parameterization of the effective radius of ice free clouds for use in global climate models. *Atmos. Res.*, **27**, 305-339

- Borovikov, A.M. and Mazin, I.P. 1975 Microphysical properties of clouds. In: *Aviation-climate atlas-handbook of USSR. Part 2*. Dubrovina L.S., Eds. Moscow, Gidrometeoizdat, 127-148
- Brenguier, J.-L. and W. W. Grabowski, 1993: Cumulus entrainment and cloud droplet spectra: A numerical model within a two-dimensional dynamical framework. *J. Atmos. Sci.*, **50**, 120-136.
- Cober, S.G., Isaac, G.A. and Strapp, J.W. 2001 Characterizations of aircraft icing environments that include supercooled large drops. *J. Appl. Meteor.* **18**, 515-528
- Deepak, A., and Box, M. A. 1978a Forward scattering corrections for optical extinction measurements in aerosol media. 1: Monodispersions. *Applied Optics*, **17**, 2900-2908
- Deepak, A., and Box, M. A. 1978b Forward scattering corrections for optical extinction measurements in aerosol media. 1: Polydispersions. *Applied Optics*, **17**, 3169-3176
- Feigelson, E. M., 1978 Preliminary radiation model of a cloudy atmosphere. Part I: Structure of clouds and solar radiation. *Beirt. Phys. Atmos.*, **51**, 203-229
- Federal Aviation Administration, 1999 U.S. Code of Federal Regulations, Title 14 (Aeronautics and Space), Part 25 (Airworthiness Standard: Transport Category Airplanes), Appendix C, National Archives and Records Administration, U.S. Government Printing Office, Washington D.C.
- Fouquart, Y., Buries, J. C., Herman, M. and Kandel R. S. 1990 The influence of clouds on radiation: A climate-modelling perspective. *Rev. Geoph.*, **28**, 145-166
- Gultepe, I. and Isaac G.A. 1997 Liquid water content and temperature relationship from aircraft observations and its applicability to GCMs. *J. Climate*, **10**, 446-452
- Gultepe, I. and Isaac G.A., 1999 Scale effects on the relationship between cloud droplet and aerosol number concentrations: Observations and models. *J. Climate*, **12**, 1268-1279
- Gultepe, I., Isaac G.A. and Cober S. G. 2001 Ice crystal number concentration versus temperature. Accepted to International J. of Climate.
- Gumprecht, R. O. and Sliepevich, C.M. 1953 Scattering light by large spherical particles. *J. Phys. Chem.* **57**, 90-95
- Han, Q., Rossow, W.B. and Lacis, A.A. 1994 Near-global survey of effective droplet radii in liquid water clouds using ISCCP data. *J. Climate*, **7**, 465-497
- Hansen J. E., and Travis, L. D. 1974 Light scattering in planetary atmospheres. *Space Sci. Rev.*, **16**, 527-610 *International Cloud Atlas (Volume II)*, 1956 WMO, Cobas, Switzerland, pp.212
- Isaac, G.A., 1991 Microphysical characteristics of Canadian Atlantic storms. *Atmos. Res.*, **26**, 339-360
- King, W. D., Parkin, D. A. and Handsworth, R. J. 1978 A hot-wire water device having fully calculable response characteristics. *J. Appl. Meteor.*, **17**, 1809-1813
- Korolev, A. V., Strapp, J. W., Isaac, G. A. and Nevzorov, A. N. 1998 The Nevzorov airborne hot wire LWC/TWC probe: principle of operation and performance characteristics. *J. Atmos. Ocean. Technol.*, **15**, 1495-1510
- Korolev, A. V., Strapp, J. W., Isaac, G. A. and Nevzorov, A. N. 1999a In situ measurements of effective diameter and effective concentration. *J. Geoph. Res.*, **104**, D4, 3993-4003
- Korolev, A.V., G.A. Isaac, and J. Hallett, 1999b Ice particle habits in Arctic clouds. *Geophys. Res. Let.*, **26**, 1299-1302
- Korolev, A.V, Isaac, G.A. and J. Hallett, 2000 Ice particle habits in stratiform clouds. *Q. J. Roy. Meteor. Soc.*, **126**, 2873-2902
- Kosarev, A. L., Mazin, I. P., Nevzorov, A. N., and Shugaev, V. F., 1976 Optical density of clouds. *Trudi TsAO\**, **124**, 5-167
- Lawson R.P., Korolev, A.V., Cober, S.G., Huang, T., Strapp, J.W. and Isaac, G.A. 1998 Improved measurements of the drop size distributions of a freezing drizzle event. *Atmos. Res.* **48**, 181-191
- Lewis, W., 1951 Meteorological aspects of aircraft icing. *Compendium of Meteorology*, American Meteorological Society, Boston, 1197-1203.
- Lohmann, U. and Feichter, J. 1997 Impact of sulfate aerosols on albedo and lifetime of clouds: A sensitivity study with the ECHAM4 GCM. *J. Geophys. Res.*, **102**, 13,685-13,700
- Manual on the Observation of Clouds and Other Meteors (Volume I)*, 1975 WMO-No407, Geneva, Switzerland, pp155

---

\* *Transactions of Central Aerological Observatory* ( in Russian)

- Martin, C. M, D. W. Johnson, and Spice A. 1994 The measurements and parameterisation of effective radius of droplets in warm stratocumulus clouds, *J. Atmos. Sci.*, **51**, 1823-1842
- Mazin, I.P., 1989 Cloud microstructure. In: *Clouds and cloudy atmosphere (Handbook)*, Mazin I.P., and A.Kh. Khrgian, Eds. Leningrad, Gidrometeoizdat, 297-341
- Mazin, I.P., 1995 Cloud water content in continental clouds of middle latitudes. *Atmos. Res.*, **35**, 283-297
- Mazin, I.P. and Minervin, V.E. 1993 Regulation of terminology in cloud physics. *Russian Meteorology and Hydrology (Allerton Press, New York)*, **4**, 1-8
- Mazin, I.P., Monachova N.A. and Shugaev, V.F. 1996 Vertical distribution of water content and optical characteristics of continental stratiform clouds. *Russian Meteorology and Hydrology (Allerton Press, New York)*, **9**, 9-25
- Mazin, I.P., Nevzorov, A.N. and Shugaev, V.F. 1983 The light attenuation parameters of clouds of different types. *Soviet Meteorology and Hydrology (Allerton Press, New York)*, **9**, 31-36
- McClatchey, R.A., Fenn, R.W., Selby, J.E.A., Volz, F.E. and Garing, J.S. 1972 Optical properties of the atmosphere. 3rd ed., Environmental Research Paper, No 411, AFCRL-72-0497, [NTIS N7318412], Bedford, Massachusetts
- McFarlane, N.A., Boer, G.J., Blanchet, J. P. and Lazare, M. 1992 The Canadian Climate Centre second-generation general circulation model and its equilibrium climate. *J. Climate*, **7**, 1013-1044
- Minervin, V.E., 1954 Experimental measurements of water content in stratiform clouds clouds. *Trudi TsAO\**, **14**, 130-138
- Mitchell, J. F. B., Davis, R. A., Ingram, W. J. and Senior, C. A. 1995 On surface temperature, greenhouse gases, and aerosols: Models and observations. *J. Climate*, **8**, 2364-2386
- Nevzorov, A.N., 1971 Evaluation of the effect of the forward scattering in measurements of the transparency of clouds. *Trudi TsAO\**, **102**, 102-117
- Nevzorov, A. N., 1983: Aircraft cloud water content meter. *Trudi TsAO\**, **147**, 19-26
- Nevzorov A. N., and Shugaev, V. F. 1972 The use of integral parameters for study of cloud microstructure. *Trudi TsAO\**, **101** 32-47
- Nevzorov A. N. and Shugaev, V. F. 1974 Aircraft cloud extinction meter. *Trudi TsAO*, **106** 3-10
- Nevzorov, A. N. 1980 Aircraft cloud water content meter. *Comm. a la 8eme Conf. Int. sur la Phys. des Nuages, Clermont-Ferrand, France*, v. II, 701-703
- Oreopoulos, L. and Barker, H. W. 1999 Accounting for subgrid-scale cloud variability in a multi-layer, 1D solar radiative transfer algorithm. *Q. J. R. Meteorol. Soc.*, **125**, 301-330
- Pruppacher, H. R. and Klett, J. D. 1997 *Microphysics of Clouds and Precipitation*. Kluwer Academic Publisher, London
- Pincus, R. and S. Klein, 2000: Unresolved spatial variability and process rates in large scale models. *J. Geophys. Res.*, **105**, 27,059-27,065.
- Sand, W.R., Cooper, W.A., Politovich, M.K. and Veal, D.L. 1984 Icing conditions encountered by a research aircraft. *J. Climate Appl. Meteor.*, **23**, 1427-1440
- Shifrin K.M. 1988 *Physical optics of ocean water*. Amer. Inst. of Physics, New York, pp285
- Stephens, G.L., 1978: Radiation profiles in extended water clouds. II: Parameterization schemes. *J. Atmos. Sci.*, **35**, 2123-2332.
- Stephens, G. L. 1984 The parameterization of radiation for numerical weather prediction and climate models. *Mon. Weather Rev.*, **112**, 826-867
- Slingo, A. 1989 A GCM parameterization for the shortwave radiative properties of water clouds. *J. Atmos. Sci.*, **46**, 1419-1427
- Sundqvist, H., 1979 A parameterization scheme for non-convective condensation including prediction of cloud water content. *Q. J. R. Meteorol. Soc.*, **104**, 677-690
- Tiedtke, M. 1993 Representation of clouds in large-scale models. *Mon. Weather Rev.*, **121**, 3040-3061
- van de Hulst, H. C. 1957 *Scattering of light by small particles*. Wiley, New York
- Volkovitsky, O.A., Pavlova, L.N. and Petrushin, A.G. 1984 *Optical properties of the ice clouds*. Gidrometeoizdat, pp198
- Wood, R. 2000 Parameterization of the effect of drizzle upon the droplet effective radius in stratocumulus clouds. *Q. J. R. Meteorol. Soc.*, **126**, 3309-3324

**TABLE 1.** LENGTH OF CLOUDS FOR DIFFERENT CLOUD TYPES AND TEMPERATURE INTERVALS IN LCP CLOUD ARCHIVE

Temperature (°C)	St, Sc (km)	Ns (km)	As,Ac (km)	Ci (km)	Cu (km)	Haze (km)	All types (km)	$\Delta x$ (km)
0<T<+10°C	2842	3019	917	0	954	69	7802	0.54
-10<T<0°C	8610	17879	12572	0	1786	134	40980	0.56
-20<T<-10°C	1088	4911	13747	0	311	53	20110	0.61
-30<T<-20°C	0	431	8992	4202	129	196	13950	0.68
-40<T<-30°C	0	0	1647	7246	85	0	8978	0.73
-50<T<-40°C	0	0	198	3011	0	0	3209	0.77
-50<T<+10°C	12540	26239	38074	14459	3264	452	95028	

**TABLE 2** MEDIAN VALUES OF TOTAL WATER CONTENT ( $TWC$ ), EXTINCTION COEFFICIENT ( $\beta$ ), EFFECTIVE DIAMETER ( $D_{EFF}$ ), AND EFFECTIVE CONCENTRATION ( $N_{EFF}$ ) FOR DIFFERENT TEMPERATURE INTERVALS

Temperature (°C)	$TWC$ (gm <sup>-3</sup> )	$\beta$ (km <sup>-1</sup> )	$D_{eff}$ (μm)	$N_{eff}$ (cm <sup>-3</sup> )
0oC<T<+10oC	0.16	31	16	95
-10oC<T<0oC	0.10	11	21	22
-20oC<T<-10oC	0.048	5	23	6
-30oC<T<-20oC	0.021	2.5	20	4
-40oC<T<-30oC	0.011	2	15	7
-50oC<T<-40oC	0.007	1.5	18	4

**TABLE 3** CORRELATION COEFFICIENTS  $K_{\beta W}$ ,  $K_{WD}$ ,  $K_{\beta D}$  FOR DIFFERENT TEMPERATURE INTERVALS.

Temperature	$K_{\beta W}$	$K_{WD}$	$K_{\beta D}$	Length (km)	Nbr. Points
0oC<T<+10oC	0.69	0.23	-0.29	8007	14770
-10oC<T<0oC	0.57	0.34	-0.34	41384	73020
-20oC<T<-10oC	0.55	0.48	-0.22	20193	32932
-30oC<T<-20oC	0.63	0.65	-0.02	14006	20643
-40oC<T<-30oC	0.69	0.80	0.24	8978	12350
-50oC<T<-40oC	0.55	0.85	0.18	3209	4145

**TABLE 4** MEDIAN VALUES OF TOTAL WATER CONTENT ( $TWC$ ), EXTINCTION COEFFICIENT ( $\beta$ ), EFFECTIVE DIAMETER ( $D_{EFF}$ ), AND EFFECTIVE CONCENTRATION ( $N_{EFF}$ ) FOR DIFFERENT CLOUD TYPES

Cloud type	$TWC$ ( $gm^{-3}$ )	$\beta$ ( $km^{-1}$ )	$D_{eff}$ ( $\mu m$ )	$N_{eff}$ ( $cm^{-3}$ )
St,Sc	0.11	30	12	145
Cu	0.15	25	17	62
Ns	0.10	9	26	7
As,Ac	0.05	4.5	22	6
Ci	0.01	2.2	16	5
Haze	0.015	2	24	2

**TABLE 5** CORRELATION COEFFICIENTS  $K_{\beta W}$ ,  $K_{WD}$ ,  $K_{\beta D}$  FOR DIFFERENT CLOUD TYPES.

Cloud type	$K_{\beta W}$	$K_{WD}$	$K_{\beta D}$	Length (km)	Nbr. Points
St,Sc	0.75	0.22	-0.24	12540	23073
Cu	0.71	0.25	-0.27	3264	5697
Ns	0.60	0.36	-0.30	26239	45919
As,Ac	0.58	0.48	-0.20	38074	59775
Ci	0.71	0.73	0.17	14459	19008
Haze	0.85	0.75	0.47	452	710

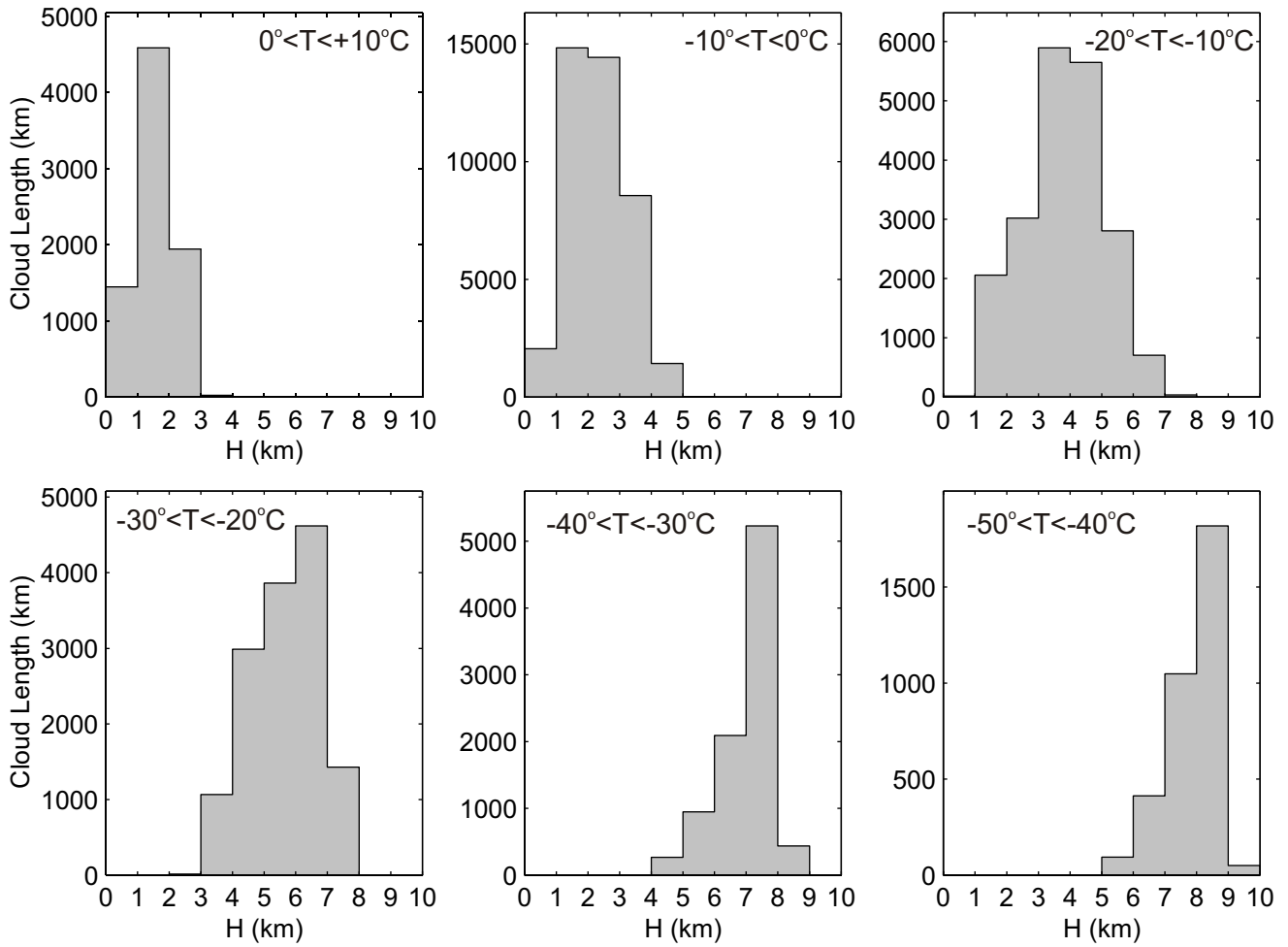


**Figure 1.** Length of in-cloud measurements versus altitude for different temperature intervals.

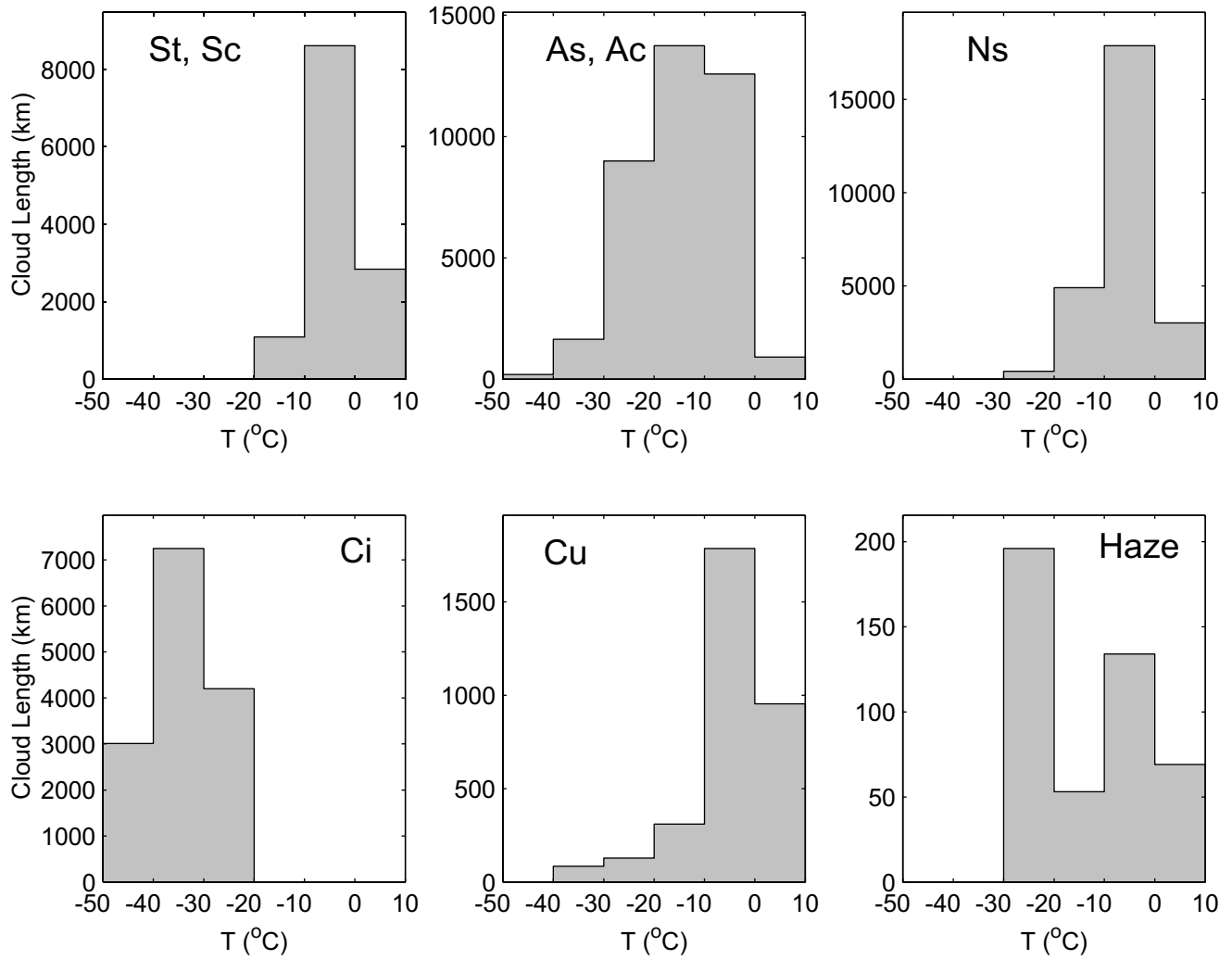


**Figure 2.** Length of in-cloud measurements versus temperature for different cloud types.

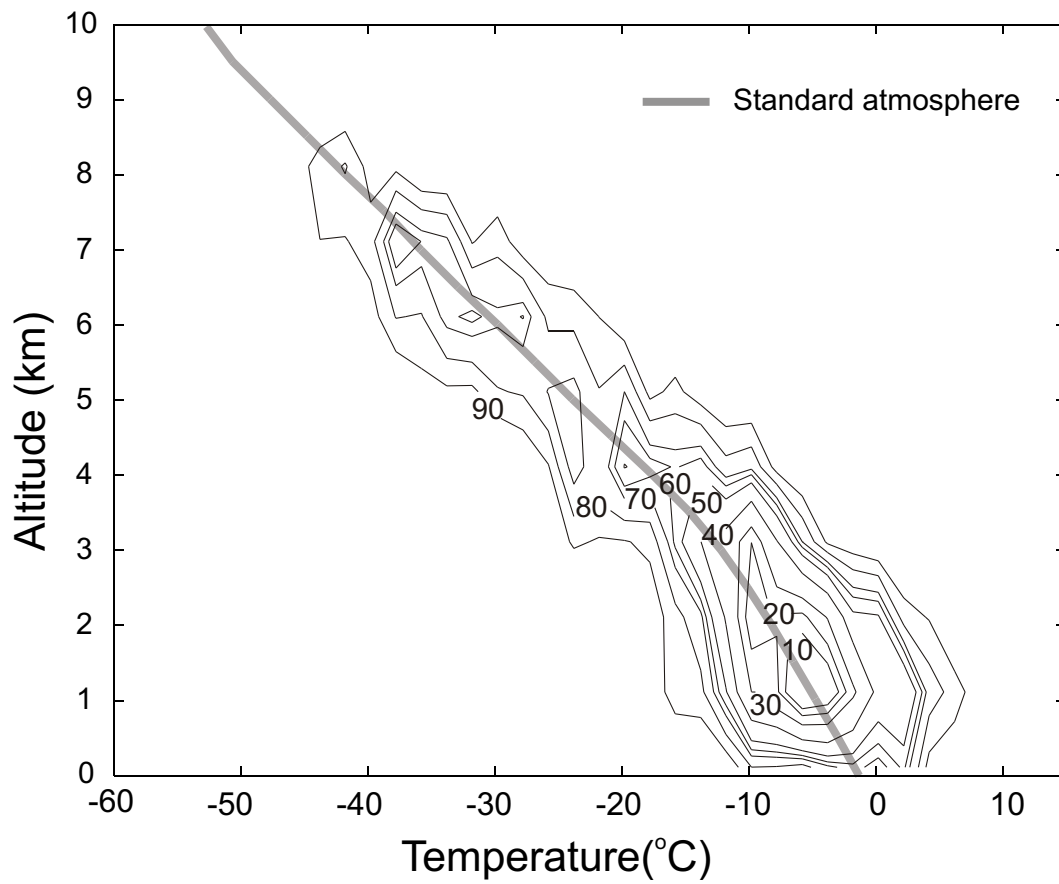


**Figure 3.** Dependence of measured cloud temperature on altitude. The solid line is the standard atmosphere for mid latitudes for a winter season (McClatchey et al. 1972).

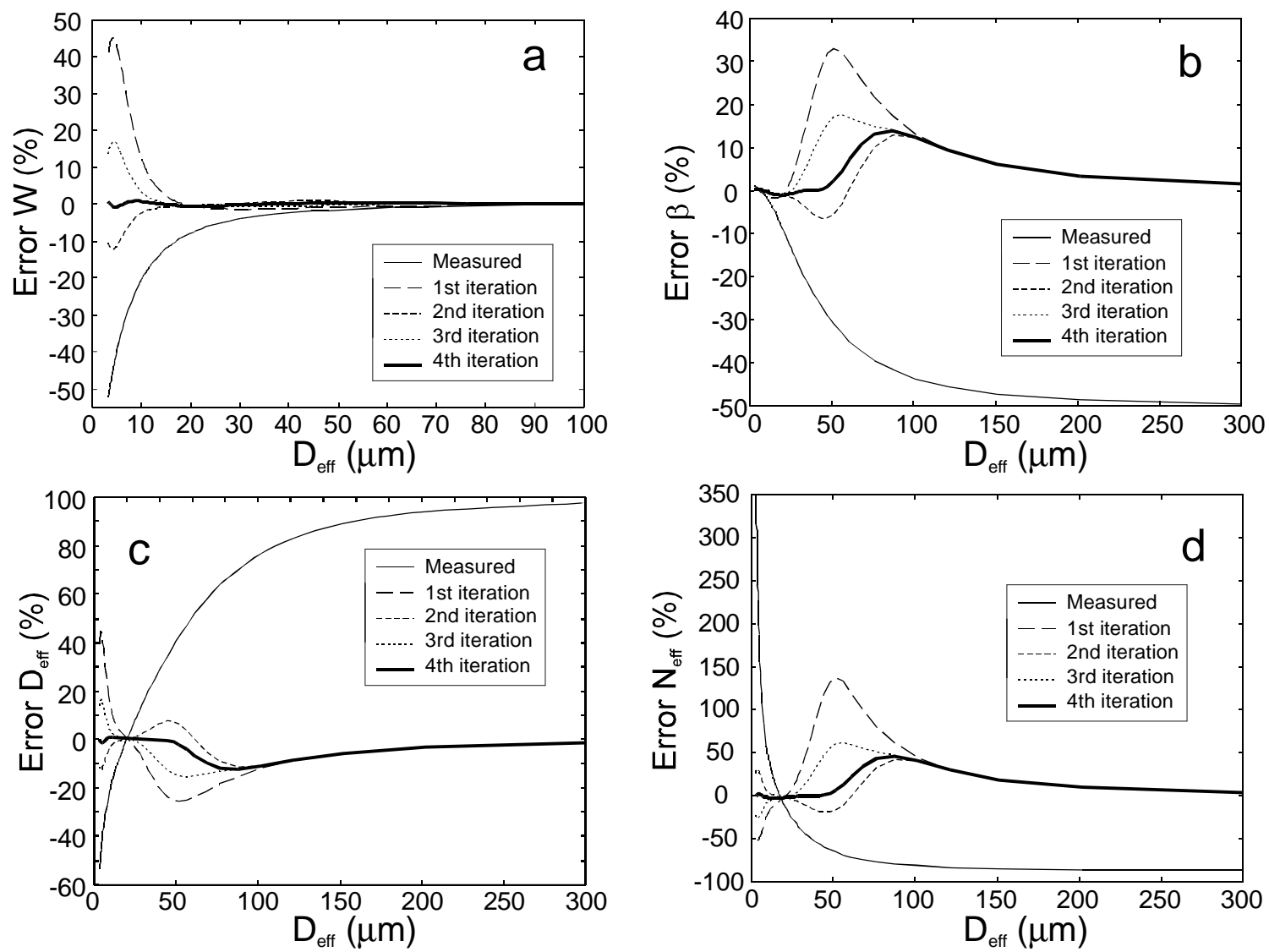


**Figure 4.** Relative errors for measured and retrieved (a) total water content, (b) extinction coefficient, (c) effective diameter, and (d) effective concentration versus actual effective diameter. The droplet size spectrum was assumed to be a gamma distribution (see text).

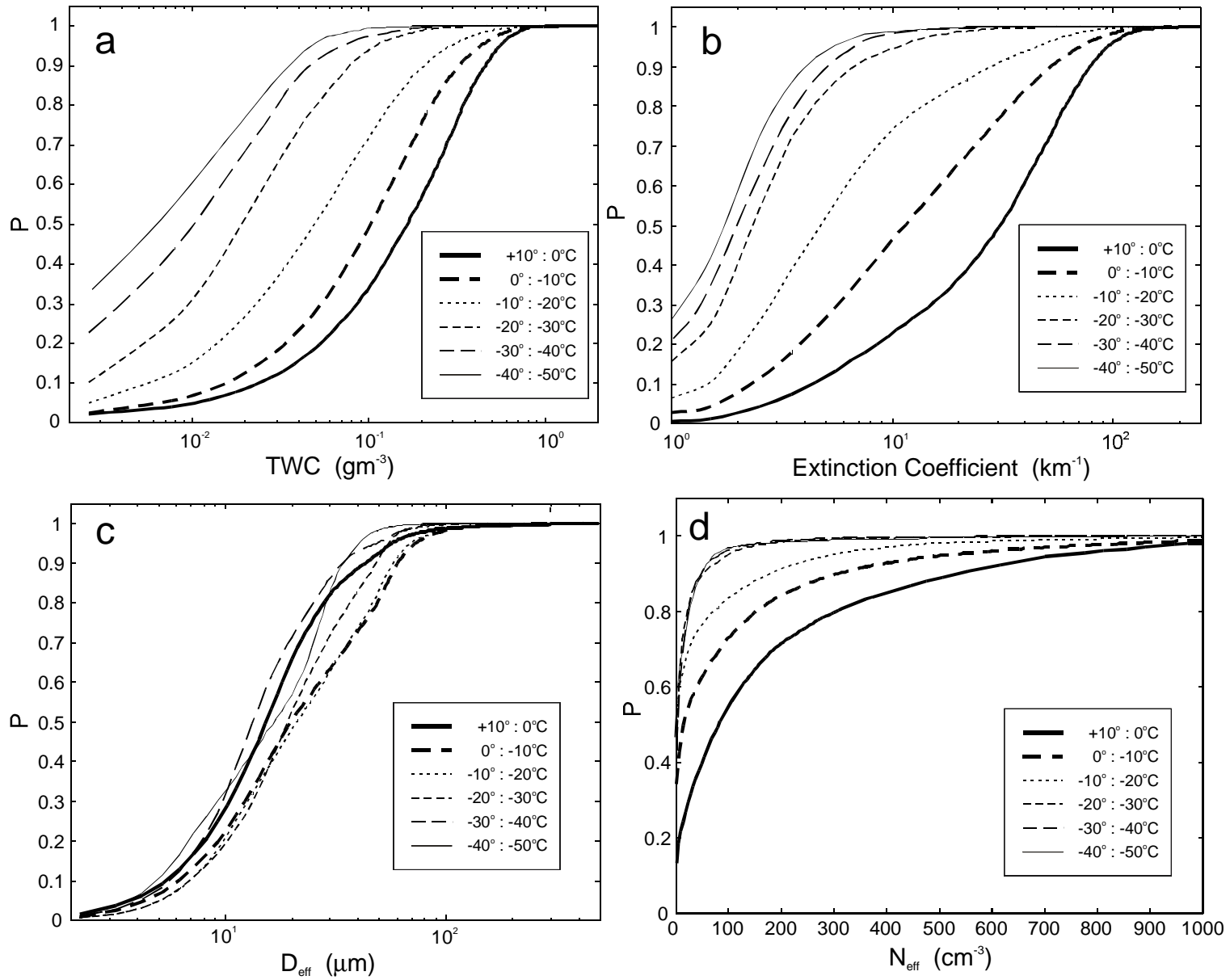


**Figure 5.** Cumulative probability distributions of (a) total water content, (b) extinction coefficient, (c) effective diameter, and (d) effective concentration for different temperature intervals.

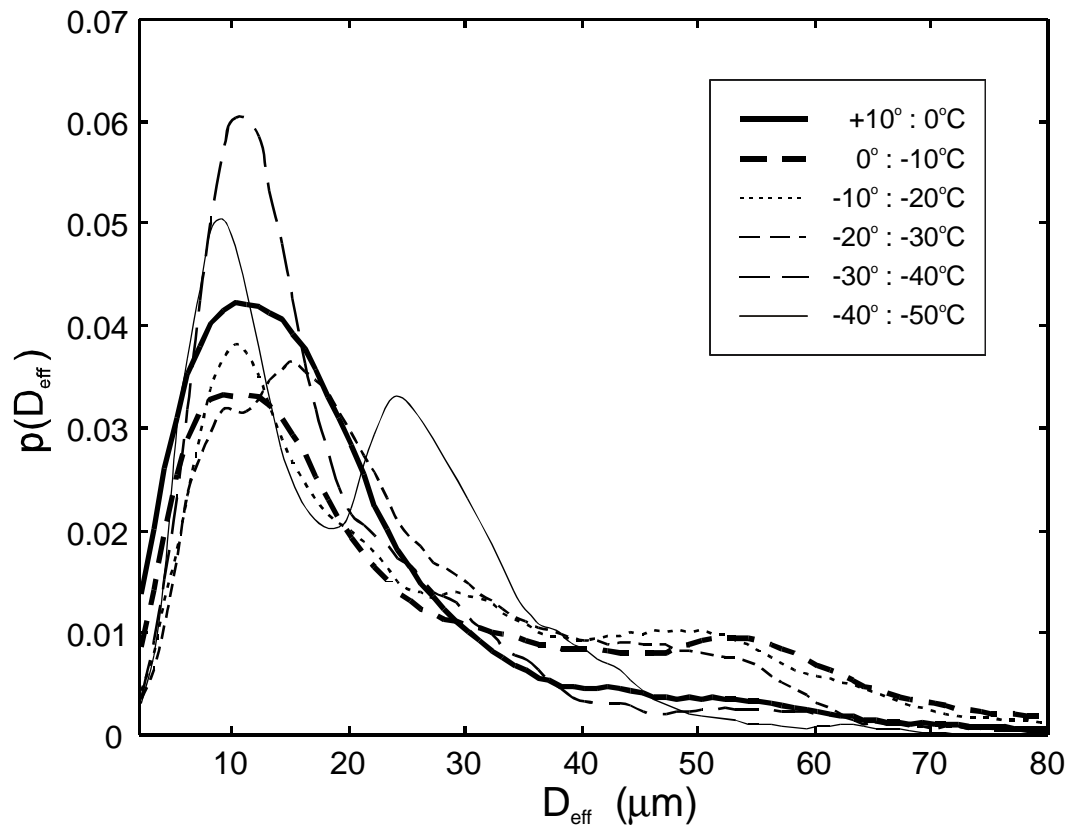


**Figure 6.** Density frequency distributions of effective diameter for different temperature intervals.

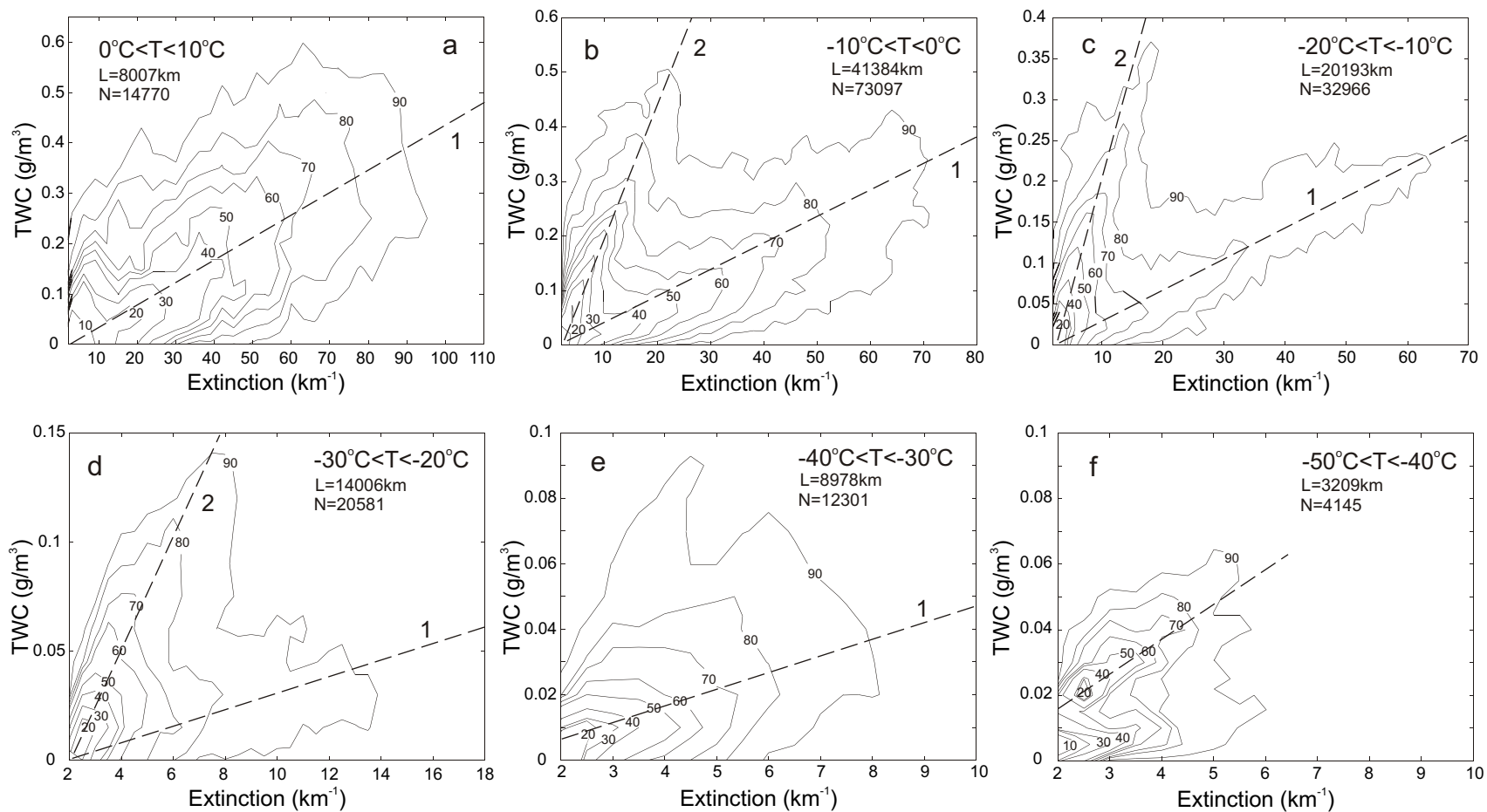


**Figure 7.** Scatter diagrams of total water content versus extinction coefficient for different temperature intervals. The numbers in the upper corners denote temperature intervals, the length of in-cloud measurements ( $L$ ), and the number of sampling points ( $N$ ) attributed to the temperature interval.

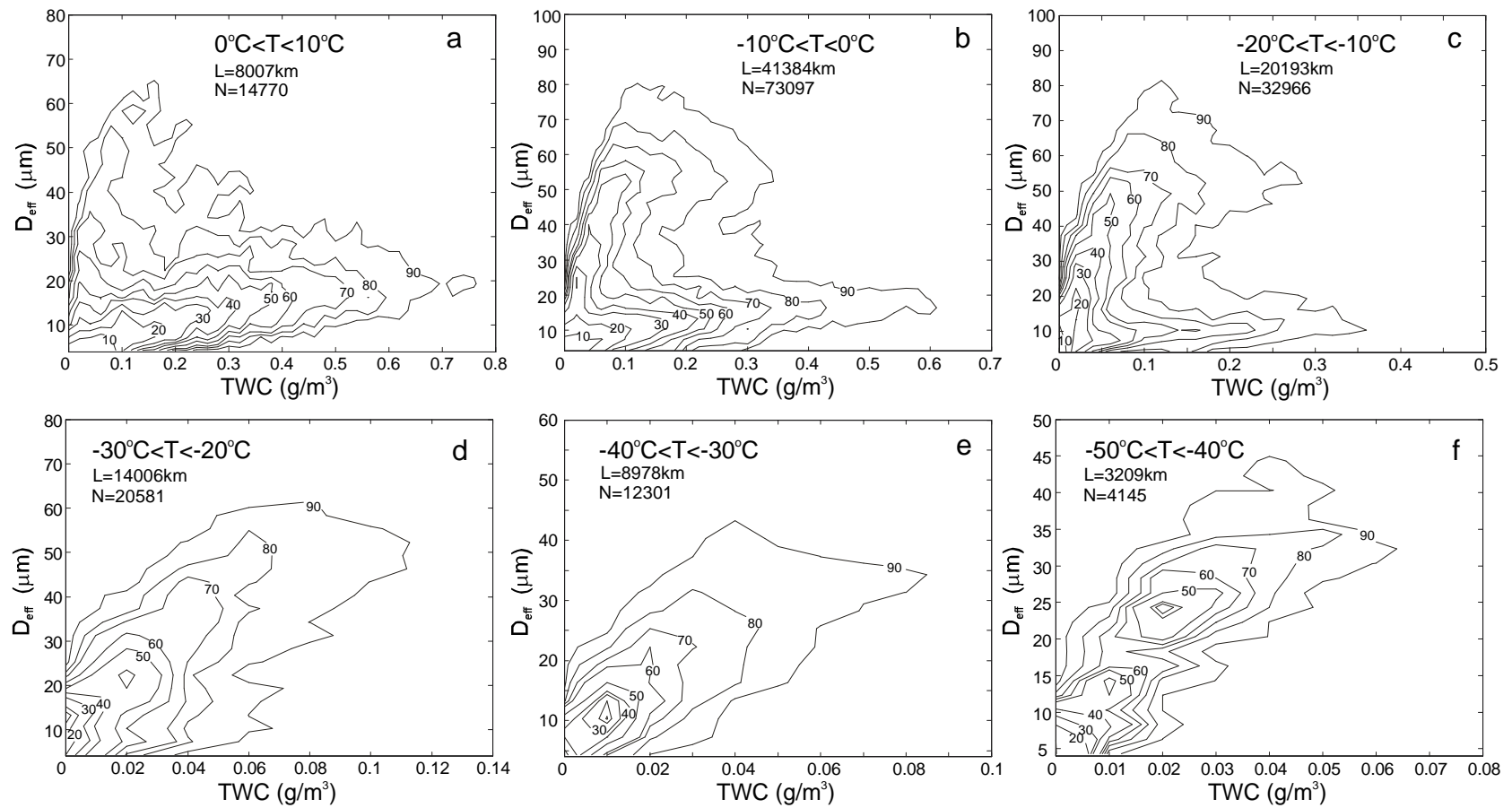


**Figure 8.** As in Fig. 7. Scatter diagrams of effective diameter versus total water content for different temperature intervals.

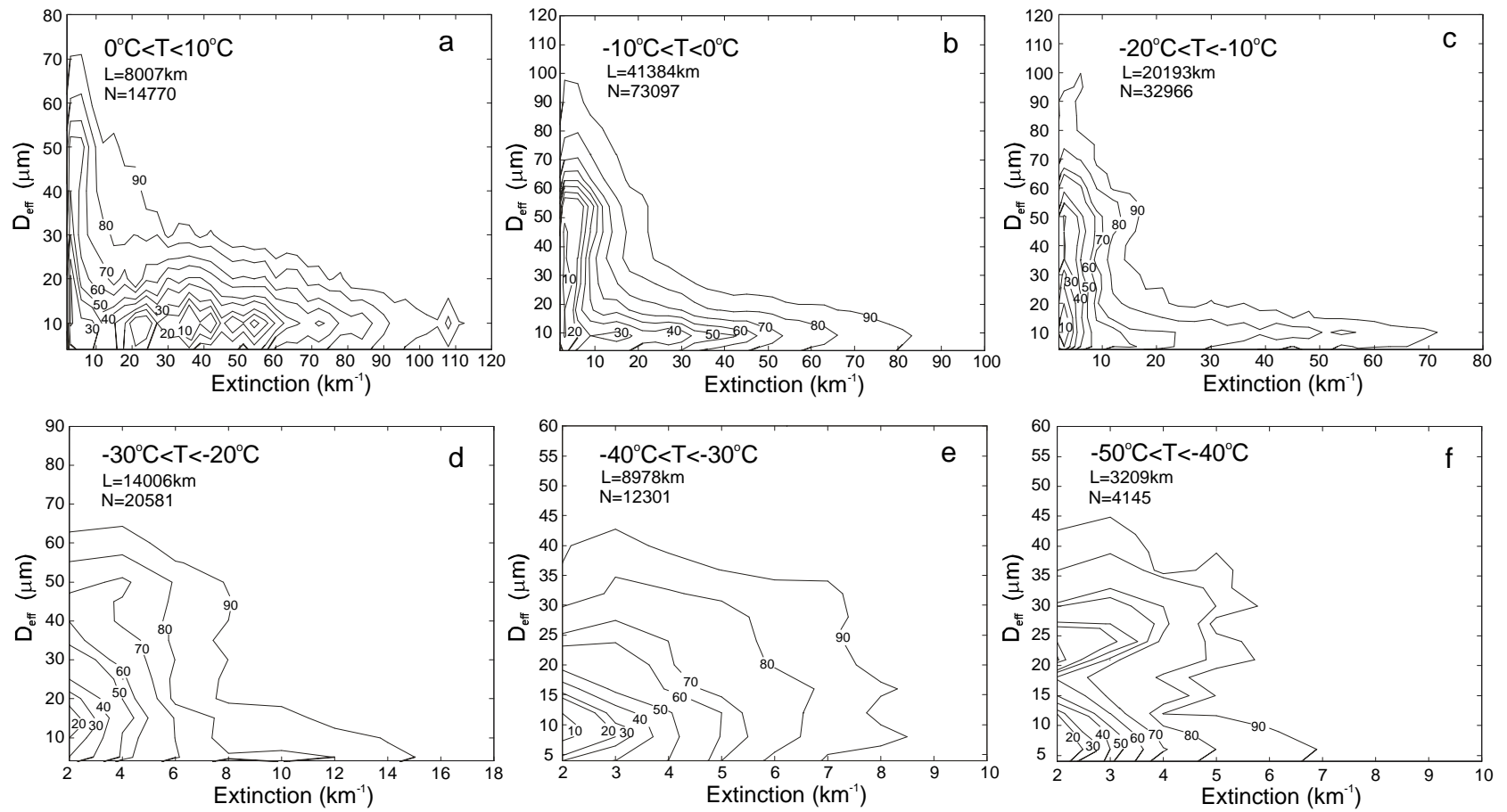


**Figure 9.** As in Fig. 7 except for effective diameter versus extinction coefficient.

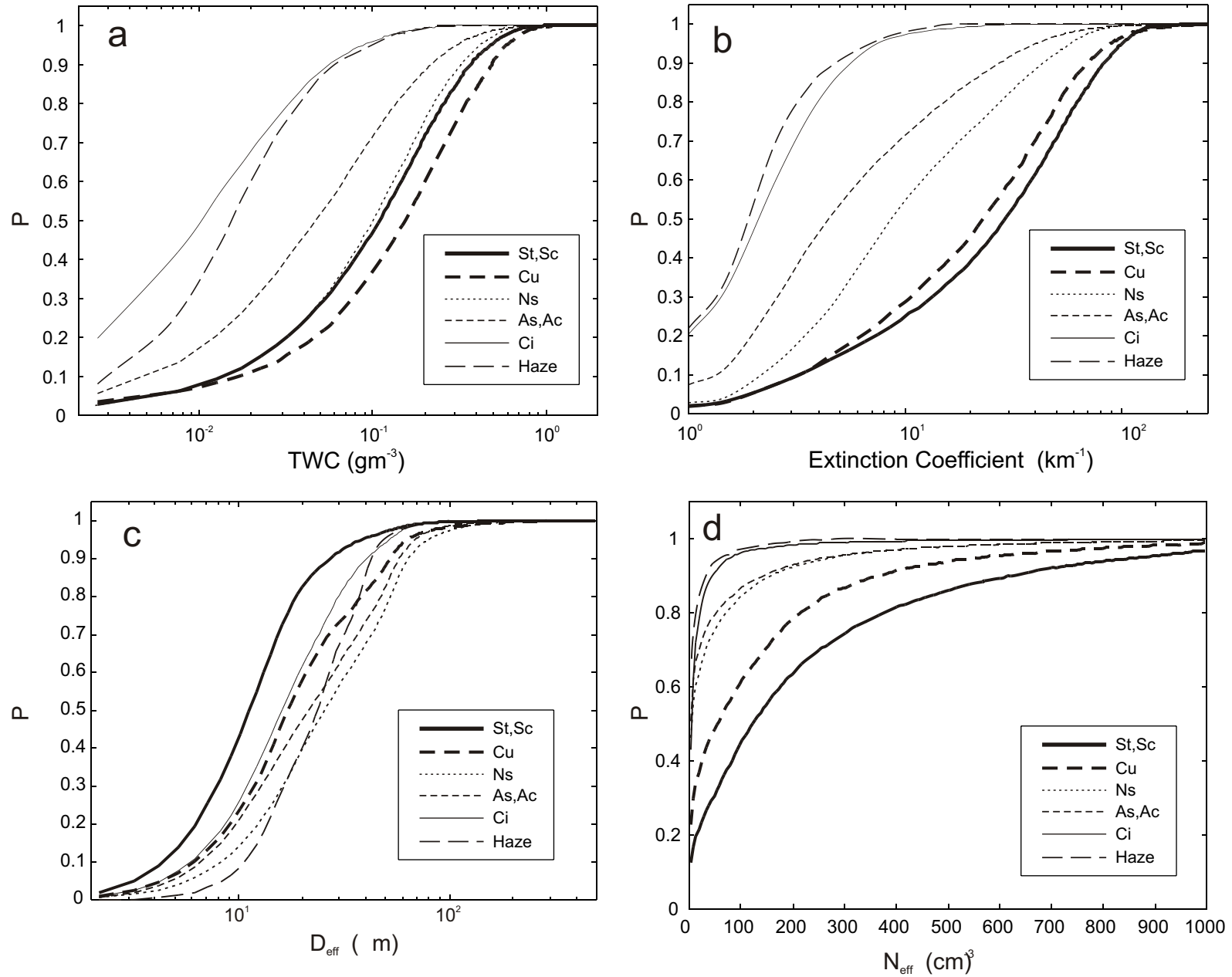


**Figure 10.** Cumulative probability distributions of (a) total water content, (b) extinction coefficient, (c) effective diameter, and (d) effective concentration for different cloud types.

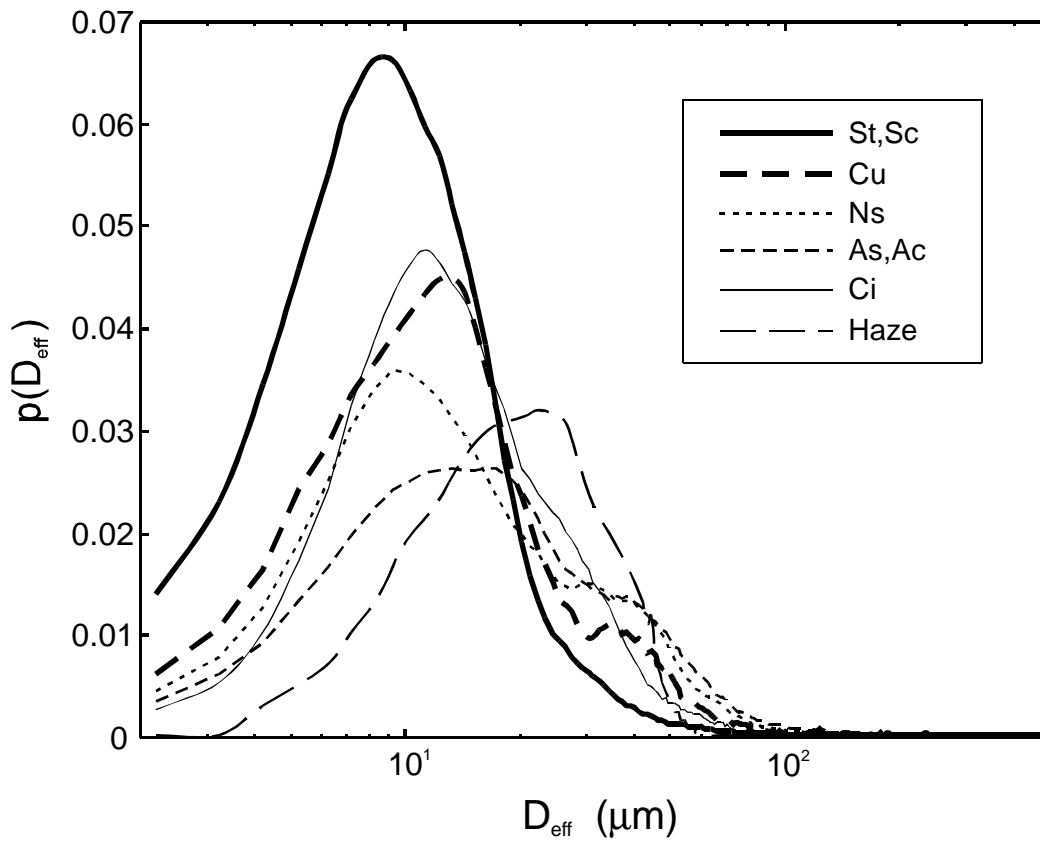


**Figure 11.** Density frequency distributions of effective diameter for different cloud types.

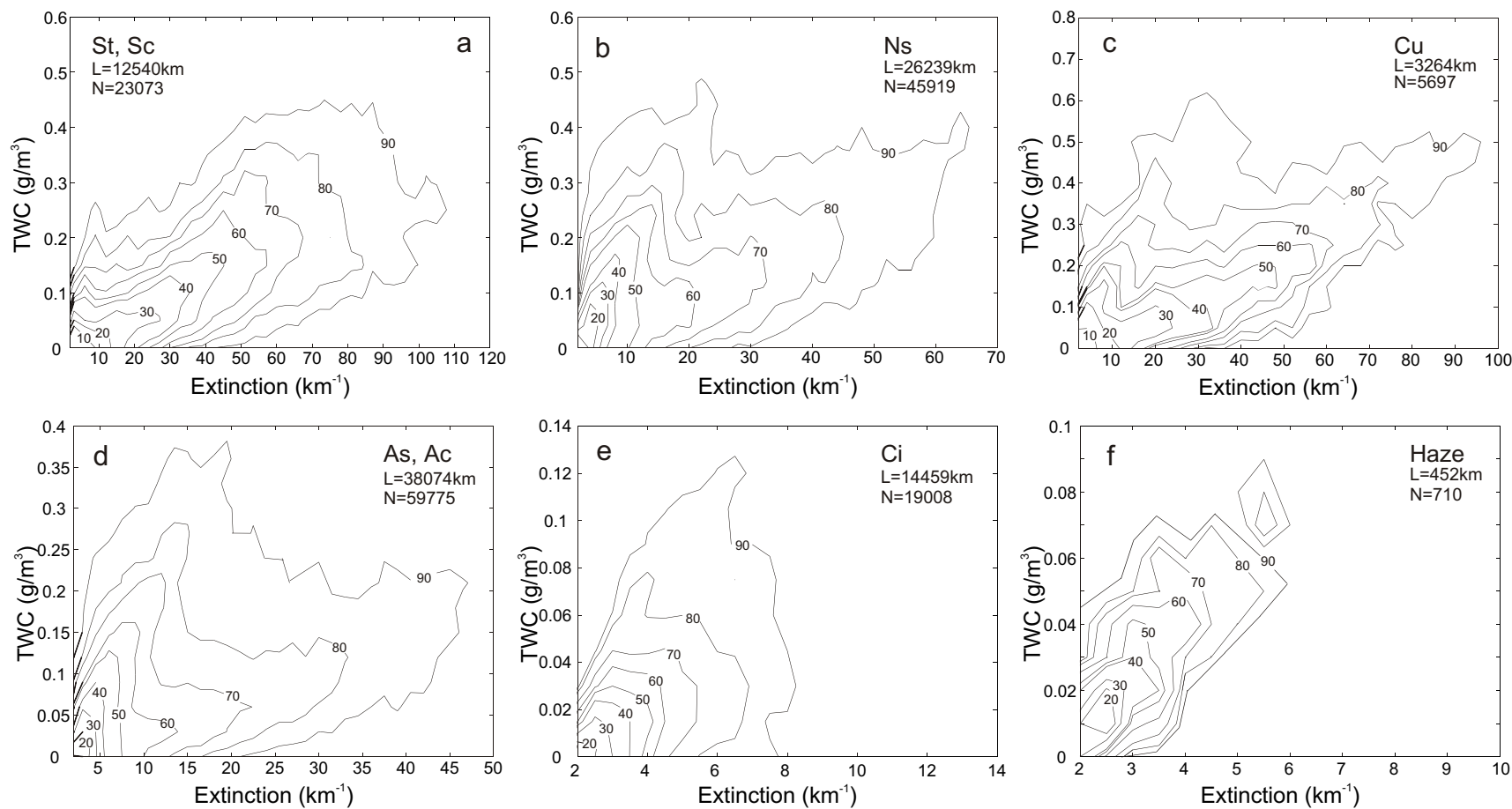


**Figure 12.** Scatter diagrams of total water content versus extinction coefficient for different cloud types. The numbers in the upper corners denote the length of in-cloud measurements ( $L$ ), and number of sampling points ( $N$ ) attributed to the cloud types.

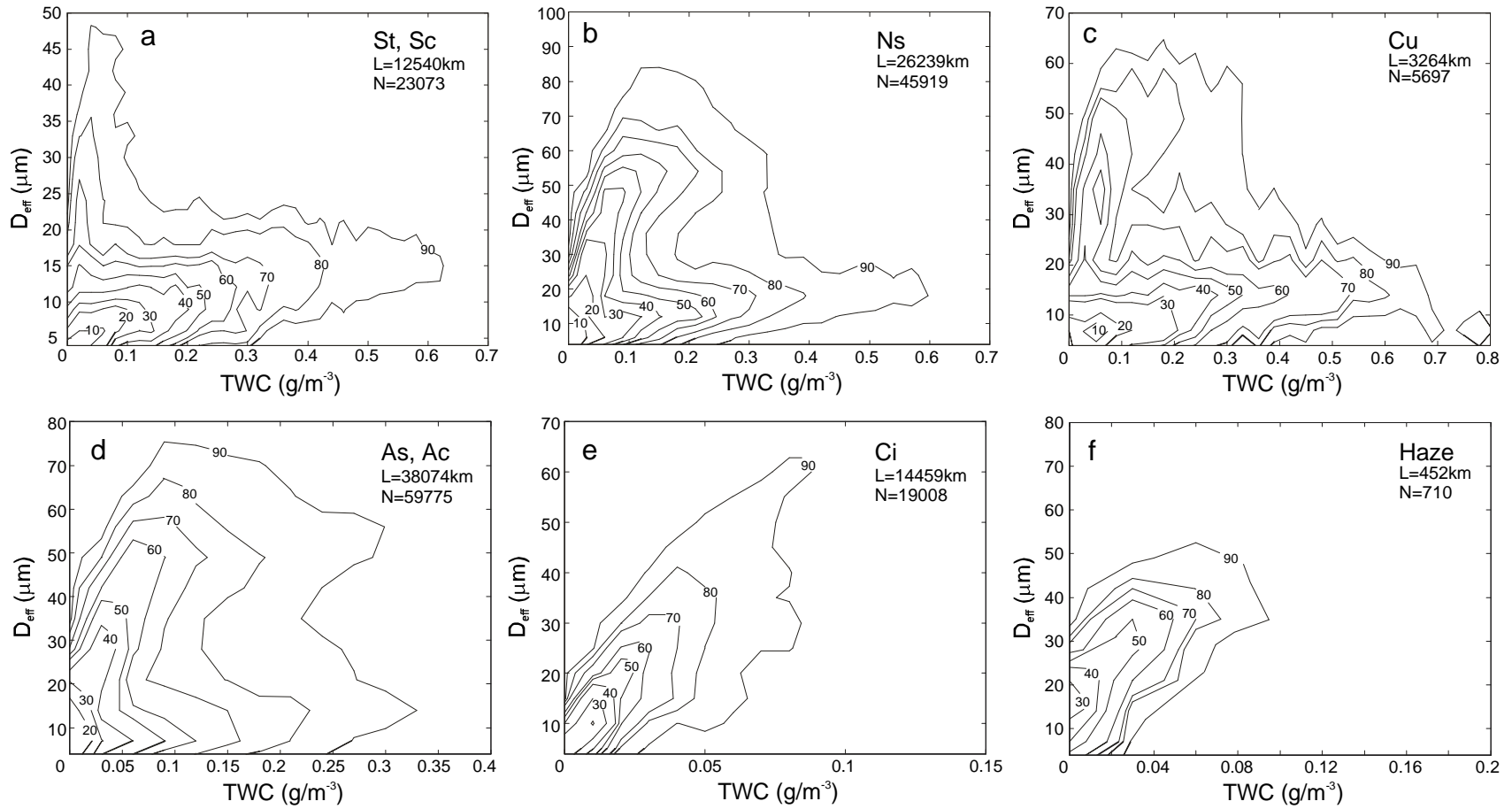


**Figure 13.** As in Fig. 12. Scatter diagrams of the effective diameter versus total water content for different cloud types.

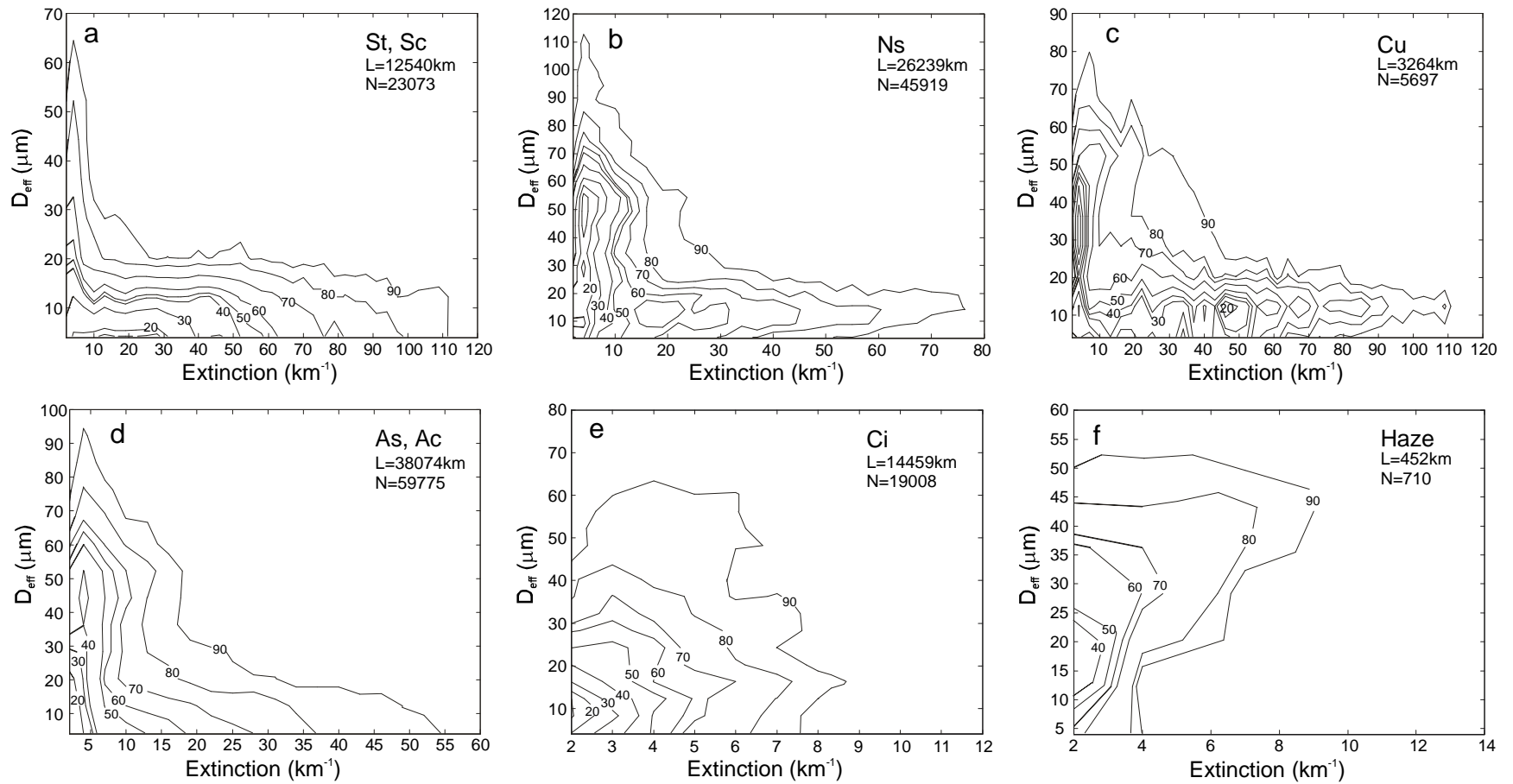


**Figure 14.** As in Fig. 12. Scatter diagrams of the effective diameter versus total water content for different cloud types.

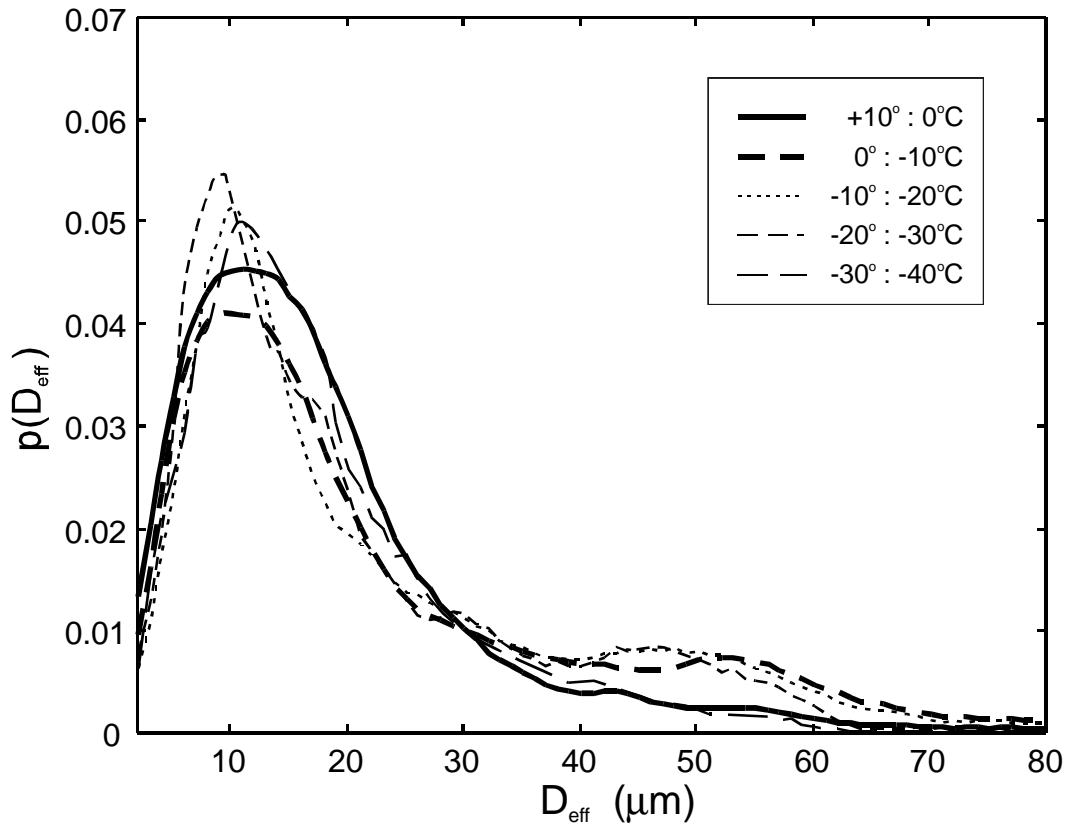


**Figure 15.** Density frequency distributions of effective diameter for different temperature intervals. The calculation of  $D_{\text{eff}}$  was conducted for  $W_{th} = 0.005 \text{ gm}^{-3}$  and  $\beta_{th} = 5 \text{ km}^{-1}$ .

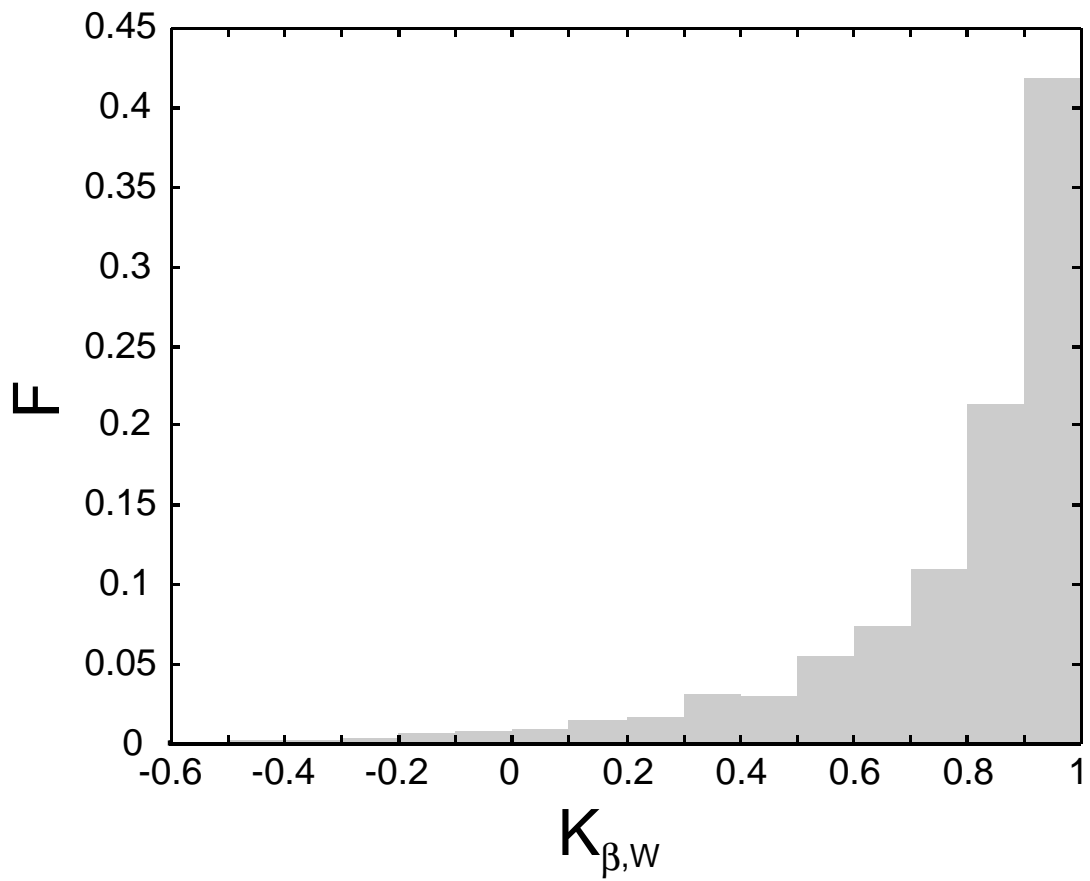


**Figure 16.** Frequency of occurrence of the correlation coefficient between  $W$  and  $\beta$  for the clouds included in the archive.

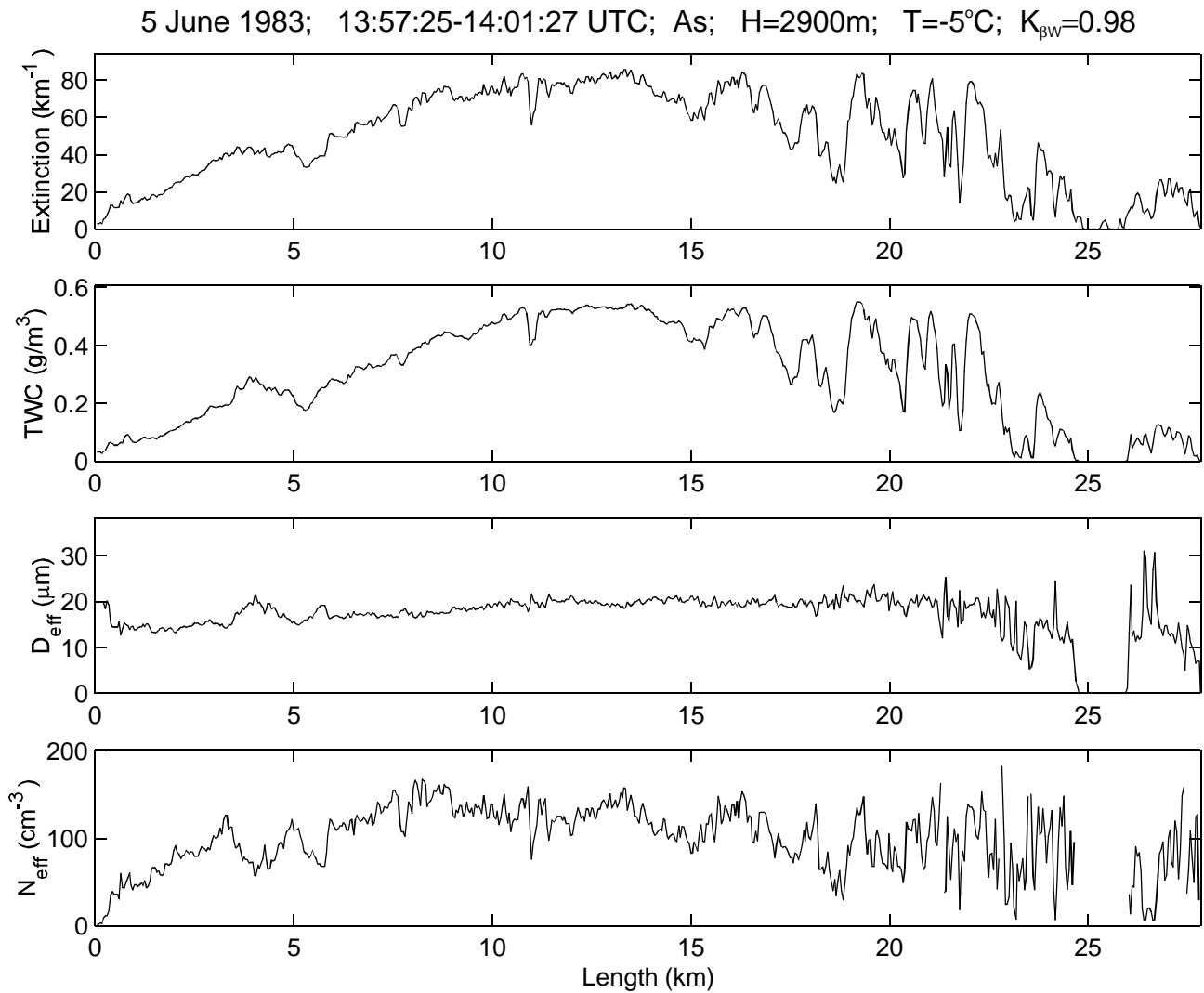


**Figure 17.** Variations of (a) extinction coefficient, (b) total water content, (c) effective diameter, and (d) effective concentration in altostratus. This cloud exhibits a high correlation between  $W$  and  $\beta$ ;  $K_{\beta W}=0.98$ .

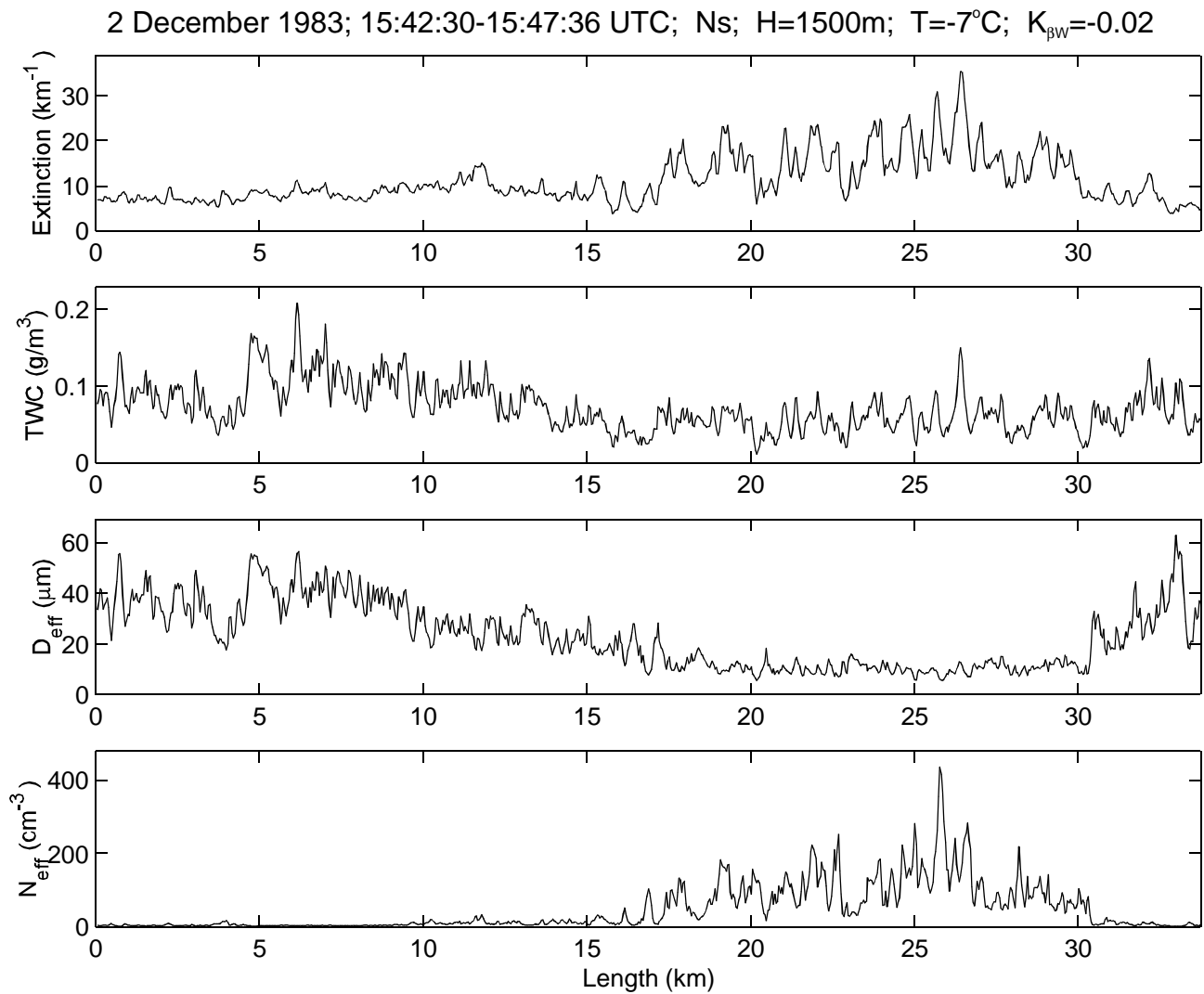


**Figure 18.** Variations of (a) extinction coefficient, (b) total water content, (c) effective diameter, and (d) effective concentration in nimbostratus. This cloud exhibits a low correlation between  $W$  and  $\beta$ ;  $K_{\beta W}=-0.02$ .